# $CO_2$ and $H_2S$ Corrosion in Oil Pipelines

Master Thesis

of

Mythili Koteeswaran

University of Stavanger

Faculty of Mathematics and Natural Science

June 2010

University of Stavanger

# Faculty of Science and Technology

# MASTER'S THESIS

| | |
|---|---|
| Study program/ Specialization:<br><br>Masters of Science in Environmental Technology / Water Science | Spring semester, 2010<br><br>Open / ~~Restricted~~ access |
| Writer:<br>Mythili Koteeswaran | .....<br>(Writer's signature) |
| Faculty supervisor: Tor Hemmingsen<br><br>External supervisor(s): | |
| Title of thesis:<br><br>$CO_2$ and $H_2S$ Corrosion in Oil Pipelines | |
| Credits (ECTS): 30 | |
| Key words:<br>$CO_2$ Corrosion, $H_2S$ Corrosion, Galvanic Corrosion, Linear Polarization Resistance, Tafel | Pages: 79<br>+ enclosure: 2 CDs<br><br>Stavanger, 14.06.2010 |

# Abstract

This study has been conducted to find the corrosion behavior and corrosion rates of carbon steel in the presence of $CO_2$ and $H_2S$ at various pH levels using classical electrochemical techniques. It was found that in a galvanic coupling, the metal in the sulfide environment gets protection even at pH 3, and the bare metal which is in neutral pH was corroding sacrificially. The linear polarization resistance measurements and potentiodynamic scan of the metal without the galvanic coupling show a high degree of corrosion at pH 3. The corrosion rate generally was higher for $CO_2$/$H_2S$ system than for $H_2S$ system.

# Acknowledgement

I would like to express my sincere gratitude to Prof. Tor Hemmingsen for his continuous academic and moral support. This thesis work is a tribute to his exceptional guidance and mentorship.

I would like to acknowledge my indebtedness to Tor Gulliksen, for helping me making the galvanic cell and the samples.

I would like to acknowledge my indebtedness to Ola Risvik for helping me in getting the SEM pictures.

I would like to thank Liv Margareth Aksland for her support in the laboratory work.

I also would like to acknowledge Koteeswaran Paulpandian for his priceless suggestions and recommendations in preparing the thesis report.

# TABLE OF CONTENTS

## List of Figures

# List of Tables

# 1. INTRODUCTION

Corrosion of steel by CO2 and $CO_2$ /$H_2S$ has been one of the major problems in the oil industry since 1940. Recently, it has again come to the fore because of the technique of $CO_2$ injection for enhanced oil recovery and exploitation of deep natural gas reservoirs containing carbon dioxide[1]. The presence of carbon dioxide, hydrogen sulphide ($H_2S$) and free water can cause severe corrosion problems in oil and gas pipelines. Internal corrosion in wells and pipelines is influenced by temperature, $CO_2$ and $H_2S$ content, water chemistry, flow velocity, oil or water wetting and composition and surface condition of the steel. A small change in one of these parameters can change the corrosion rate considerably. In the presence of $CO_2$, the corrosion rate can be reduced substantially under conditions when corrosion product, iron carbonate ($FeCO_3$) can precipitate on the steel surface and form a dense and protective corrosion product film. This occurs more easily at high temperature or high pH in the water phase. When corrosion products are not deposited on the steel surface, very high corrosion rates of several millimetres per year can occur. When $H_2S$ is present in addition to $CO_2$, iron sulphide (FeS) films are formed rather than $FeCO_3$. This protective film can be formed at lower temperature, since FeS precipitates much easier than $FeCO_3$. Localised corrosion with very high corrosion rates can occur when the corrosion product film does not give sufficient protection, and this is the most feared type of corrosion attack in oil and gas pipelines.

Extensive studies had been done for $CO_2$ corrosion and $H_2S$ corrosion, but there is very little understanding of the corrosion behaviour in the presence of both the species. Hence, the objective of this project is to analyse the electrochemical behaviour of carbon steel in the presence of both $CO_2$ and $H_2S$.

In order to fulfil this objective, classical electrochemical techniques like galvanic effect, polarization techniques and electrochemical impedance spectroscopy are used to find the corrosion rates in the $CO_2$/$H_2S$ environment. The experiment is performed at room temperature and at different pH.

# 2. LITERATURE REVIEW

## 2.1. $CO_2$ Corrosion

Carbon dioxide ($CO_2$) corrosion is one the most studied form of corrosion in oil and gas industry. This is generally due to the fact that the crude oil and natural gas from the oil reservoir / gas well usually contains some level of $CO_2$. The major concern with CO2 corrosion in oil and gas industry is that $CO_2$ corrosion can cause failure on the equipment especially the main downhole tubing and transmission pipelines and thus can disrupt the oil/gas production. The basic $CO_2$ corrosion reaction mechanisms have been well understood and accepted by many researchers through the workdone over the past few decades. The major chemical reactions include $CO_2$ dissolution and hydration to form carbonic acid as shown in equations (1) and (2),

$$CO_{2(g)} \rightarrow CO_{2(aq)} \quad (1)$$

$$CO_2 + H_2O \rightarrow H_2CO_3 \quad (2)$$

The carbonic acid then dissociates into bicarbonate and carbonate in two steps as in equations (3) and (4),

$$H_2CO_3 \rightarrow H^+ + HCO_3^- \quad (3)$$

$$HCO_3^- \rightarrow H^+ + CO_3^{2-} \quad (4)$$

$CO_2$ corrosion is an electrochemical reaction with the overall reaction given in equation (5)

$$Fe + CO_2 + H_2O \rightarrow FeCO_3 + H_2 \quad (5)$$

Thus, $CO_2$ corrosion leads to the formation of a corrosion product, $FeCO_3$, which when precipitated could form a protective or a non-protective scale depending on the environmental conditions [2].

The electrochemical reactions at the steel surface include the anodic dissolution of iron as given in equation (6)

$$Fe \rightarrow Fe^{2+} + 2e^- \quad (6)$$

The cathodic reactions are proton reduction reaction and the direct reduction of carbonic acid as in equations (7) and (8)

$$2H^+ + 2e^- \rightarrow H_2 \quad (7)$$

$$2H_2CO_3 + 2e^- \rightarrow H_2 + 2HCO_3^- \quad (8)$$

Despite more than three decades of intense research, it is still not known which of the two reactions (7) and (8) actually occur on the metal surface. Hence, the net cathodic current was assumed to be the sum of the currents of the two cathodic reactions. It has been suggested that the direct reduction of bicarbonate ion becomes important at higher pH [3].

### 2.1.1 The effect of pH

pH is the indication of the $H^+$ concentration in the solutions, which is one of the main species involved in the cathodic reaction of $CO_2$ process. It has been illustrated both experimentally and computationally that corrosion rate changes significantly with respect to pH. Higher pH leads to a decreased solubility of iron carbonate and thus results in an increased precipitation rate, faster formation of protective films and hence reduction of the corrosion rate.

### 2.1.2 The effect of temperature

Temperature accelerates all processes involved in $CO_2$ corrosion including transport of species, chemical reactions in the bulk of the solutions and electrochemical reactions at the metal surface. The growth of iron carbonate film is a very slow and a temperature dependent process. Increasing the temperature increases the precipitation rate of iron carbonate significantly. Depending on the solubility of protective films, temperature can either increase or decrease the corrosion rate[4]. In the case of corrosion where protective films do not form (typically at low pH), corrosion rate increases with increase in temperature. However, at a higher pH increased temperature would accelerate the kinetics of precipitation and facilitate protective film formation, thus decreasing the corrosion rate.

## 2.2. $H_2S$ Corrosion

The internal corrosion of carbon steel in the presence of hydrogen sulfide represents a significant problem for both oil refineries and natural gas treatment facilities. Surface scale formation is one of the important factors governing the corrosion rate. The scale growth depends primarily on the kinetics of scale formation. In contrast to relatively straight forward iron carbonate precipitation in pure $CO_2$ corrosion, in an $H_2S$ environment many types of iron sulfide may form such as amorphous ferrous sulfide, mackinawite, cubic ferrous sulfide, smythite, greigte, pyrrhotite, troilite and pyrite, among which mackinawite is considered to form first on the steel surface by a direct surface reaction[5]. The poorly known mechanism of $H_2S$ corrosion makes it difficult to quantify the kinetics of iron sulfide scale formation.

A probable mechanism for Iron dissolution in aqueous solutions containing $H_2S$ based on the formation of mackinawite film, as proposed by Sun et al[6] is shown in figure 1.

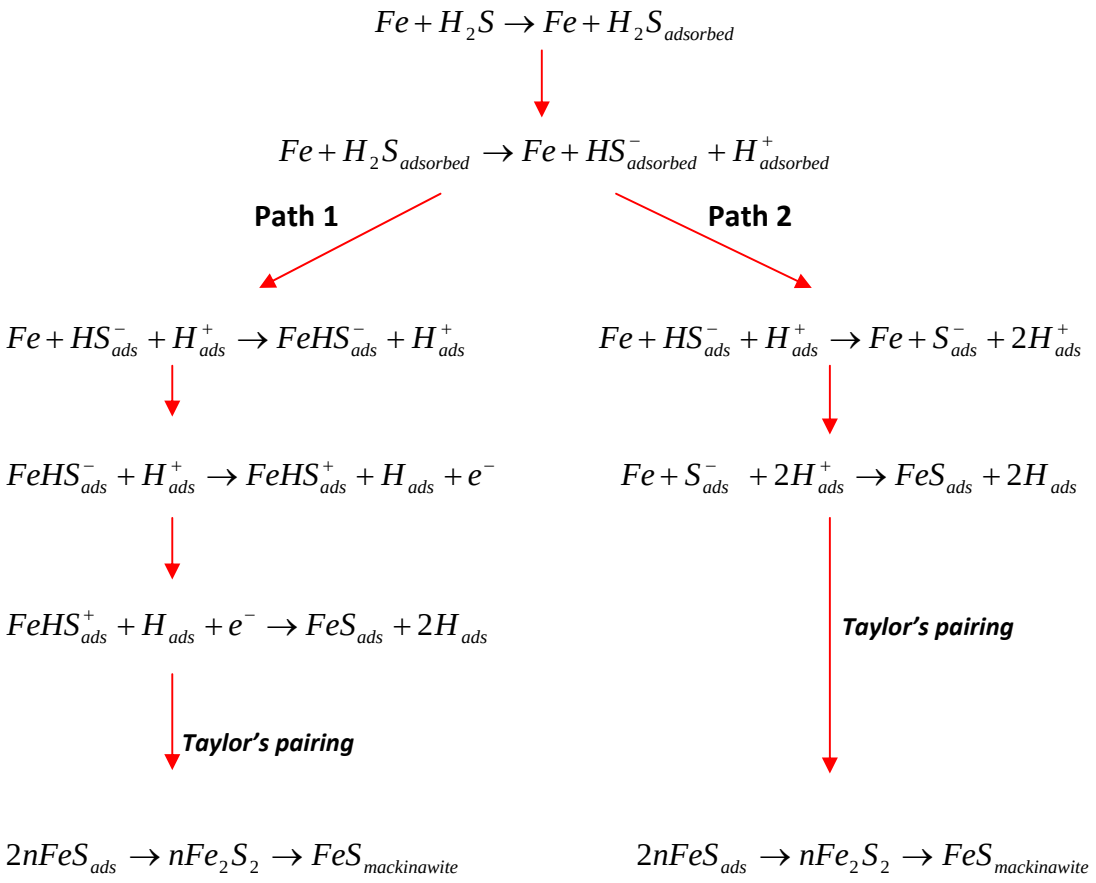


Figure1. Proposed mechanism of $H_2S$ corrosion on Fe.

### 2.2.1. The effect of pH

The protective nature and composition of the corrosion product depend greatly on the pH of the solution. At lower values of pH (<2), iron is dissolved and iron sulfide is not precipitated on the surface of the metal due to a very high solubility of iron sulfide phases at pH values less than 2. In this case, $H_2S$ exhibits only the accelerating effect on the dissolution of iron. At pH values from 3 to 5, inhibitive effect of $H_2S$ is seen due to the formation of ferrous sulfide (FeS) protective film on the electrode surface [7].

### 2.2.2. The effect of $H_2S$ Concentration

$H_2S$ concentration has an immense influence on the protective ability of the sulfide film formed. As the concentration of $H_2S$ increases, the film formed is rather loose even at pH 3-5 and does not contribute to the corrosion inhibiting effect[8].

### 2.2.3. The effect of temperature

The temperature dependence of $H_2S$ corrosion is very weak for short term exposure and does not seems to have an effect at longer exposure times. This suggest that the corrosion rate is predominantly controlled by the presence of iron sulfide scale[5].

## 2.3. $CO_2$/$H_2S$ Corrosion

The internal corrosion of mild steel in the presence of both $CO_2$ and $H_2S$ represents a significant problem for oil and gas industries. Although the interaction of $H_2S$ with low carbon steels have been published by various authors, the understanding of the effect of $H_2S$ on $CO_2$ corrosion is still limited because the nature of the interaction with carbon steel is complicated.

In the presence of $H_2S$, additional chemical reactions occurring in the bulk of the solution include:

Dissociation of dissolved $H_2S$ is given in equation (9).

$$H_2S \xrightarrow{K_{H2S}} H^+ + HS^- \qquad (9)$$

where $K_{H_2S} = \dfrac{[H^+][HS^-]}{[H_2S]}$

The dissociation of $HS^-$ ion is given by equation 10.

$$HS^- \xrightarrow{K_{HS^-}} H^+ + S^{2-} \quad (10)$$

where $K_{HS^-} = \frac{[H^+][S^{2-}]}{HS^-}$

$H_2S$ gas is about three times more soluble than $CO_2$ gas, the acid created by the dissociation of $H_2S$ is about three times weaker than carbonic acid[9]. Hence, the effect of $H_2S$ gas on decreasing the solution pH is approximately the same as $CO_2$ gas. Unlike dissolved $CO_2$, dissolved $H_2S$ does not need to undergo the slow hydration step in order to become an acid.

In a $H_2S$ dominated system, $H_2S$ lower the solution pH as it acts as a weak acid like carbonic acid. It can also increase the corrosion rate in a similar way as carbonic acid, by providing an extra cathodic reaction as in equation (11)

$$H_2S + e^- \rightarrow H + HS^- \quad (11)$$

However, this direct reduction of $H_2S$ is only feasible if the amount of $H_2S$ is high enough, which means the system has to be either $H_2S$ dominated system (sour regime) or $CO_2/H_2S$ mixed system[10]. Moreover, elemental sulphur is often associated with high concentration of $H_2S$ and very little is known about the complex interactions taking place in the presence of elemental sulphur.

When hydrogen sulfide is present in low concentration in a $CO_2$ dominated system, the iron sulfide (FeS) film interferes with the formation of the carbonate scale ($FeCO_3$)[11]. This is of interest because the iron sulfide film would seem to be more easily removed from the pipe wall than the iron carbonate scale. Under turbulent conditions, removal of the protective scale will lead to an increased corrosion rate.

The kinetics of scale formation in the $CO_2/H_2S$ system is complicated and still not understood well. The makeup of the surface scale under these conditions will not only depend on the chemistry of the brine and the respective solubility of iron carbonates and iron sulfides, but also on the competitive kinetics of the two scale formation mechanisms[12].

## 2.4. Corrosion product film formation

$CO_2/H_2S$ corrosion on the metal surface is strongly dependent on the type of corrosion product film formed on the surface of the metal during the corrosion process. The precipitation rate or the formation of these films depends on various environmental factors and greatly on the concentration of species. The stability, protectiveness, and adherence of these films determine the nature and the rate of corrosion. Depending on the composition, the corrosion films can be of different forms.

### 2.4.1. Iron carbide ($Fe_3C$)

Iron carbide is an undispersed component of mild steel, which is left behind after the corrosion of iron from the steel structure. Iron carbide films are conductive electrically, very porous and non-protective[13] films can significantly affect the corrosion process by either decreasing the corrosion rate by acting as a diffusion barrier, or increasing the corrosion by increasing the active specimen surface area by forming a conductive bridge between the counter and working electrodes. Also, this kind of film formation could result in galvanic coupling of the film to the metal or acidification of the solution inside the corrosion product film which is very dangerous and by far the strongest reason that could be given for the occurrence of localized corrosion.

### 2.4.2. Iron carbonate ($FeCO_3$)

In a CO2 corrosion situation, iron carbonate is formed from the reaction of iron and carbonate ions given by equation (12)

$$Fe^{2+} + CO_3^{2-} \rightarrow FeCO_3(s) \qquad (12)$$

The rate of precipitation of iron carbonate is so slow that most often the precipitation kinetics rather than the thermodynamics come into consideration. Precipitation of solid iron carbonate occurs when the product of the concentrations of $Fe^{2+}$ and $CO_3^{2-}$ ions in the solution exceed a certain limit as the solubility limit.

The rate of precipitation of the iron carbonate ( $(R_{FeCO_{3(s)}})$ can be expressed by the equation (13) [2]

$$R_{FeCO_{3(S)}} = \frac{A}{V} \cdot f(T) \cdot Ksp_{FeCO_3} \cdot f(S_{FeCO_3}) \quad (13)$$

where A/V is the surface area to volume ratio and $Ksp_{FeCO3}$ is the solubility limit of $FeCO_3$.

The supersaturation S is defined as in equation (14)

$$S_{FeCO_3} = \frac{c_{Fe^{2+}} c_{CO_3^{2-}}}{Ksp_{FeCO_3}} \quad (14)$$

Since $CO_3^{2-}$ ion concentration is dependent on the pH, it can be deduced to eqn.15

$$S = f(Fe^{2+}, pH) \quad (15)$$

Therefore, supersaturation and temperature are the most important factors affecting the rate of precipitation, and the nature and protectiveness of the iron carbonate film. Precipitation of iron carbonate on the surface of the metal decreases the corrosion rate by acting as a diffusion barrier for the corrosive species to travel to the metal surface by blocking few areas on the steel surface and preventing electrochemical reactions from happening on the surface [14].

### 2.4.3. Iron sulfide (FeS) film

The structure and composition of the protective FeS film depends greatly on the concentration of $H_2S$ in the system. The protective nature of the film mainly depends on the pH of the solution [15]. At a solution pH value of 3 to 5, with a small concentration of $H_2S$, a protective film of FeS inhibits the corrosion rate of the metal coupon[7]. In nearly neutral pH and at room temperature, mackinawite forms through a solid state reaction, while at a pH value between 5 and 7, amorphous FeS precipitates. The kinetics of FeS formation is complicated than the iron carbonate film. The reaction for the formation of solid iron sulphide is given in equation (16).

$$Fe^{2+} + S^{2-} \Rightarrow FeS(s) \quad (16)$$

It is assumed that the precipitation of solid iron sulphide occurs when the product of the concentration of $Fe^{2+}$ and $S^{2-}$ exceed the solubility limit of FeS. The rate of precipitation of Iron sulfide is given in equation (17)

$$R_{FeS(s)} = \frac{A}{V} \cdot f(T) \cdot Ksp_{FeS} \cdot f(S_{FeS}) \quad (17)$$

Where supersaturation $S_{FeS}$ is defined in equation (18)

$$S_{FeS} = \frac{c_{Fe^{2+}} c_{S^{2-}}}{Ksp_{FeS}} \quad (18)$$

It could also be observed that the supersaturation of FeS is a strong function of the concentration of $H_2S$ and $Fe^{2+}$. At the metal surface, because of the fast depletion of $H^+$ ions, the local pH near the metal surface is greater than the bulk pH. This could result in a larger super saturation of FeS and precipitation happens even faster at the metal surface. Since iron sulfide is a semi-conductive film, precipitation of iron sulfide in combination with other kind of non-conductive film (e.g. $FeCO_3$) on the surface of the metal could decrease the corrosion rate by acting as a diffusion barrier for the corrosive species to travel towards the metal surface. If FeS is the only one material precipitating on the surface of the metal, even if the film is thick, the corrosion rate may not be low because of the conductivity of the film. Also, precipitation of only FeS on the surface could result in false depiction of corrosion rate if electrochemical techniques are used. The reason is the interference of the conductive FeS film in the process of electron transfer.

The amount of $Fe^{2+}$ has an immense influence on the formation and nature of the iron carbonate and iron sulfide scale[12]. Increased $Fe^{2+}$ concentration can lead to higher super saturation of both iron carbonate and iron sulfide according to equations (13) and (17), respectively, which could increase the precipitation rate of iron carbonate and iron sulphide. The precipitated film could be very protective by being dense and acting as a diffusion barrier to the corrosive species, or it could be porous and thick and still could not be protective. Porous and incomplete films are very hazardous to the pipe wall as they are very favorable for localized attack of the metal. Hence, porosity of the film is the most important factor in determining the corrosion rate of the film under filming conditions.

Researchers[12] have found that the corrosion products formed in $CO_2/H_2S$ system depends on the competitiveness of iron carbonate and mackinawite. At high $H_2S$ concentration and low $Fe^{2+}$ concentration, mackinawite is the predominant scale formed on the steel surface. At low $H_2S$ concentration and high $Fe^{2+}$ concentration, both iron carbonate and mackinawite are formed.

# 3. ELECTROCHEMICAL METHODS

## 3.1 Galvanic Corrosion

Galvanic corrosion, also referred to as two-metal or bimetallic corrosion, occurs when two dissimilar metals or alloys are in contact electrically while both are immersed in an electrolyte solution. One of the two metals is corroded preferentially by this type of corrosion; that is the most active or anodic metal corrodes rapidly while the more noble or cathodic metal is not damaged. Galvanic attack can be uniform in nature or localized at the junction between the alloys depending on conditions. It can be particularly severe under the condition where protective corrosion film does not form or where they are removed by condition of erosion corrosion.

Every metal or alloy has a unique corrosion potential. $E_{corr}$, when immersed in a defined corrosive electrolytic solution. Thus, when two dissimilar metals are connected in an aqueous environment, their differences in corrosion potentials will cause corrosion. The metal with the more negative potential perform oxidation and the other metal with more positive potential perform reduction. Thus, in a couple between two metals A and B, the active metal A is the anode, while the noble metal B is the cathode, with the corresponding reactions:

$$A \rightarrow A^{n+} + ne^{-} \quad (19)$$

$$B^{m+} + me^{-} \rightarrow B \quad (20)$$

Every metal has been rated for nobility and then placed on galvanic scales according to nobility. Basically nobility is an indication of the resistance to corrosion, especially of one metal contacting another metal. The relative nobility of a material can be predicted by measuring its corrosion potential. The Galvanic series rank metals and alloys in order of reactivity or electrical potential. Metals that are least noble are very anodic, electropositive or high potential and will corrode most easily, whereas metals that are more noble are highly cathodic, electronegative or low potential and will be the more resistant to corrosion. The most corrosive effects will occur between metals from the opposite ends of the galvanic scale or ranking of nobility.

Dissimilar metals in contact with each other in the presence of an electrolyte causes current to flow through their points of contact at the expense of the metal with the higher potential or less nobility. The much less noble metal is gradually consumed in the electrochemical reaction and will deteriorate or wear away as the metal ions migrate away from the very anodic metal to the more noble cathodic one. The more noble metal's corrosion resistance actually increases from this transfer of ions to it from the less noble metal, while the other metal is gradually getting consumed. Also, oxides formed on a metal surface can form a galvanic couple with the same metal with no oxide film as these two metal surface can have different potential [16].

A zero resistance ammeter (ZRA) is used to measure the galvanic coupling current between two dissimilar electrodes. ZRA is a current to voltage converter that produces a voltage output proportional to the current flowing between its two input terminals while imposing a zero voltage drop to the external circuit.

## 3.2 Linear Polarization resistance

The Linear polarization resistance method, based on electrochemical concepts, enables determination of instantaneous interfacial reaction rates such as corrosion rates and exchange current densities from a single experiment.

Whenever the potential of an electrode is forced away from its value at open-circuit, that is referred to as polarizing the electrode. When an electrode is polarized, it can cause current to flow through electrochemical reactions that occur at the electrode surface. The amount of current is controlled by the kinetics of the reactions and the diffusion of reactants both towards and away from the electrode.

In cells where an electrode undergoes uniform corrosion at open circuit, the open circuit potential is controlled by the equilibrium between two different electrochemical reactions. One of the reactions generates cathodic current and the other anodic current.

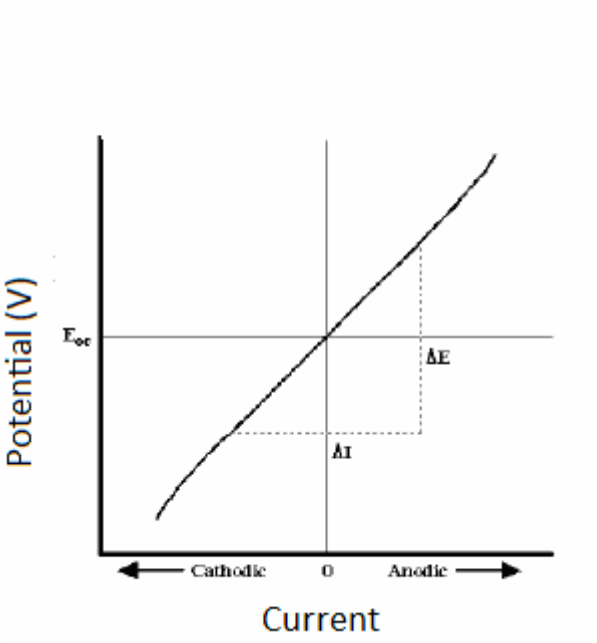


Figure2. Linear Polarization Resistance Curve.

The open circuit potential ends up at the potential where the cathodic and the anodic currents are equal. It is referred to as a mixed potential. The value of the current for either of the reactions is known as the corrosion current. When there are two simple, kinetically controlled reactions occurring, the potential of the cell is related to the current by equation (21)

$$I = I_{corr}(e^{\frac{2.303(E-Eoc)}{\beta a}} - e^{\frac{-2.303(E-Eoc)}{\beta c}}) \quad (21)$$

where,

I - measured cell current in amps,

$I_{corr}$ - corrosion current in amps,

$E_{oc}$ - open circuit potential in volts,

$\beta_a$ - anodic Beta coefficient in volts/decade

$\beta_c$ - cathodic Beta coefficient in volts/decade.

If a small signal is applied in approximation to equation (21), equation (22) can be obtained

$$I_{corr} = \frac{\beta_a \beta_c}{2.303(\beta_a + \beta_c)} \cdot (\frac{1}{R_p}) \quad (22)$$

Where, $R_p$ - polarization resistance

If the Tafel constants are known, $I_{corr}$ can be calculated from $R_p$ using equation (22). $I_{corr}$ in turn can be used to calculate the corrosion rate.

### 3.2.1 Calculation of corrosion rate from corrosion current

The corrosion current can be converted into corrosion rate by using Faraday's law

$$Q = nFM \tag{23}$$

Where

Q- charge in coulombs

n- number of electrons transferred per molecule or atom

F -Faraday's constant = 96487.7 coulombs/mole

M-number of moles.

Equation (23) can be expressed in terms of equivalent weight (EW) by using the relations EW= Atomic weight (AW)/n and M=W/AW. The expression for W, which is the mass of the electro active species, is given in equation (24)

$$W = \frac{EW \cdot Q}{F} \tag{24}$$

Modifying equation (24) gives equation (25)

$$CR = \frac{I_{corr} \cdot K \cdot EW}{d \cdot A} \tag{25}$$

CR - corrosion rate. Its units ate given by the choice of K

$I_{corr}$ - corrosion current in amperes

K - constant =3272 mm/yr

EW - equivalent weight in grams/equivalent

D - density in grams /$cm^3$

A - sample area in $cm^2$

This formula is valid only for uniform corrosion. In cases where localized corrosion occurs, this cannot be used as it gives very low corrosion rate than actually is.

## 3.3 Potentiodynamic scan

Potentiodynamic polarization is a technique where the potential of the electrode is varied at a selected rate by application of a current through the electrolyte. Through the DC polarization technique, information on the corrosion rate, pitting susceptibility, passivity, as well as the cathodic behavior of an electrochemical system may be obtained.

In a potentiodynamic experiment, the driving force (i.e., the potential) for anodic or cathodic reactions is controlled, and the net change in the reaction rate (i.e., current) is observed. The potentiostat measures the current which must be applied to the system in order to achieve the desired increase in driving force, known as the applied current. As a result, at the open circuit potential the measured or applied current will be zero.

### 3.3.1 The Anodic scan

A schematic anodic polarization curve, typical for stainless steel is illustrated in figure 2. As shown in figure 2, the scan starts from point 1 and progresses in the positive (potential) direction until termination at point 2. The open circuit potential is located at point A. At this potential the sum of the anodic and cathodic reaction rates on the electrode surface is zero. The region B is the active region, where metal oxidation is the dominant reaction taking place. Point C is known as the passivation potential, and as the applied potential increases above this value the current density is seen to decrease with increasing potential (region D), until a low, passive current density is achieved (passive region-region E). Once the potential reached a sufficiently positive value (point F, sometimes termed as breakaway potential) the applied current rapidly increases (region G). This increase may be due to a number of phenomena, depending on the alloy/environment combination. For some systems (e.g., aluminum alloys in salt water) this sudden increase in current may be pitting, while for others it may be transpassive dissolution. For some alloys, typically those with a very protective oxide, such as cobalt, the sudden increase in current is due to oxygen evolution.

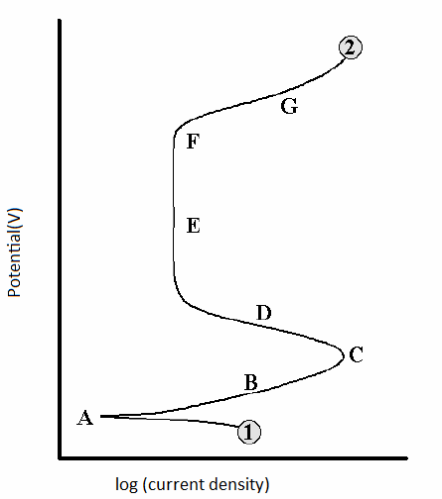


Figure 3. Theoretical anodic polarization scan on Stainless steel.

### 3.3.2 Cathodic Scan

A schematic cathodic polarization scan is illustrated in figure 4. In a cathodic potentiodynamic scan, the potential is varied from point 1 in the negative direction to point 2. The open circuit potential is located at point A. Depending on the pH and dissolved oxygen concentration in the solution, region B may represent the oxygen reduction reaction. Since this reaction is limited by how fast oxygen may diffuse in solution (mass transport controlled) there will be an upper limit on the rate of this reaction, known as limiting current density. Further decrease in the applied potential result in no change in the reaction rate, and hence the measured current remains the same (region C). Eventually, the applied potential becomes sufficiently negative for another cathodic reaction to become operative, such as illustrated at point D. As the potential, and hence driving force becomes increasingly large, this reaction may become dominant, as illustrated in region E. This additional reaction is typically the reduction of other species in the environment (such as the hydrogen evolution reaction, also known as the water reduction reaction).

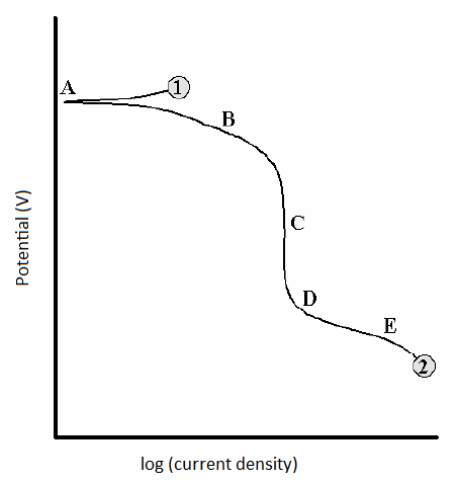


Figure 4. Theoretical cathodic polarization scan.

### 3.3.3 Corrosion rate from Potentiodynamic scan

For reactions which are essentially activation controlled, the current density can be expressed as a function of the overpotential, η, which is expressed in equation (26)

$$\eta = \beta \log \frac{i}{i_0} \tag{26}$$

Equation (26) is known as the Tafel equation, where β is the Tafel slope, i is the applied current density, and $i_0$ is the exchange current density.

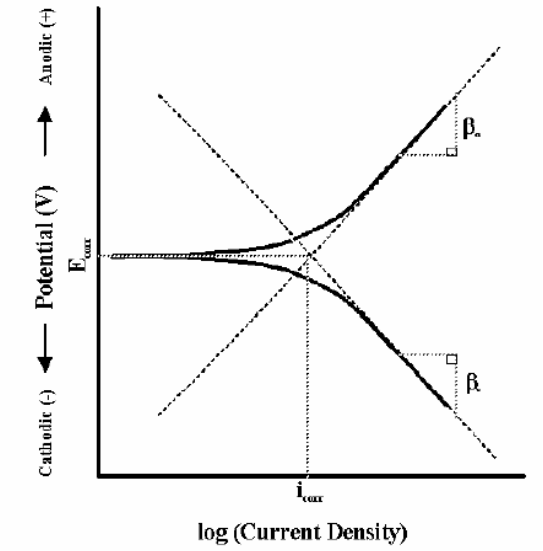


Figure 5. Tafel slope calculation.

Thus, the Tafel slope for the anodic and cathodic reactions occurring at open circuit may be obtained from the linear regions of the polarization curve, as illustrated in

figure 5. Once these slopes are established, it is possible to extrapolate back from both the anodic and cathodic regions to the point where the anodic and cathodic reaction rates (i.e., currents) are equivalent. The current density at that point is the corrosion current density ($i_{corr}$) and the potential at which it falls is the corrosion potential ($E_{Corr}$). The corrosion current density can then be used to calculate the corrosion rate using equation (25).

## 3.4 Electrochemical Impedance Spectroscopy

Alternating Current (AC) impedance or Electrochemical Impedance Spectroscopy (EIS) technique is one of the most powerful techniques for defining reaction mechanisms, for investigating corrosion process and for exploring distributed impedance system. Most generally, the application of the EIS technique has been used by researchers for the evaluation of corrosion inhibitors, anodic coatings and polymeric coatings. A brief introduction to the measurement technique is given below:

The ability of a circuit element to resist the flow of electrical current is called resistance. The resistance of an ideal resistor is defined by ohm's law as the ratio between the voltage E and current I as in equation (27)

$$R = \frac{E}{I} \tag{27}$$

An ideal resistor follows Ohm's law at all voltage and current levels and its resistance value is independent of frequency. Circuit elements which exhibit much more complex behavior are encountered in real world situations where the simple concept of ideal resistor cannot be applicable. Impedance is a more general circuit parameter which is similar to resistance in a way that it is also a measure of the ability of the circuit to resist the flow of electrical current but it is more complicated in its behavior.

Electrochemical impedance is usually measured by applying an AC potential to an electrochemical cell and measuring the current through the cell. When we apply a

sinusoidal potential excitation, the response to this potential is an AC current signal. This current signal can be analyzed as a sum of sinusoidal functions.

Electrochemical impedance is normally measured using a small excitation signal. This is done so that the cell's response is pseudo-linear. In a linear (or pseudo-linear) system, the current response to a sinusoidal potential will be a sinusoid at the same frequency but shifted in phase.

The excitation signal, expressed as a function of time, has the form as equation (28)

$$E_t = E_0 \sin(\omega t) \tag{28}$$

$E_t$ is the potential at time t, $E_0$ is the amplitude of the signal and ω is the radial frequency. The relationship between radial frequency ω (expressed in radians/second) and frequency f (expressed in hertz) is given by equation (29)

$$\omega = 2\pi rf \tag{29}$$

In a linear system, the response signal, $I_t$ is shifted in phase (ϕ) and has a different amplitude, $I_0$ as given in equation (30)

$$I_t = I_0 \sin(\omega t + \phi) \tag{30}$$

An expression analogous to Ohm's law can be used to calculate the impedance of the system as in equation (31)

$$Z = \frac{E_t}{I_t} = \frac{E_0 \sin(\omega t)}{I_0 \sin(\omega t + \phi)} = Z_0 \frac{\sin(\omega t)}{\sin(\omega t + \phi)} \tag{31}$$

Using Euler's relationship in equation (32)

$$\exp(j\phi) = \cos\phi + j\sin\phi \tag{32}$$

The impedance is then represented as a complex number as in equation (33)

$$Z(\omega) = \frac{E}{I} = Z_0(\exp(j\phi) = Z_0(\cos\phi + j\sin\phi) \tag{33}$$

Where $Z_0 = \frac{E}{I}$

The expression for impedance z is composed of both real and imaginary parts. A plot of real part of impedance on X-axis and negative of imaginary part of impedance on Y-axis is called Nyquist plot. Figure 6 shows the shape of Nyquist plot for the simple equivalent circuit with one time constant, as shown in figure 7. The impedance on the Nyquist plot can be represented as a vector of length |Z|. The angle between this vector and the X-axis is called the phase angle ϕ. The major short coming of a

Nyquist plot is that the frequency used to create a particular data point cannot be recognized. The semicircle shown in figure 6 is characteristic of a single time constant (for example, a combination of an ideal capacitance with a single resistance). EIS plots for real cases contain more than one time constant and often only portion of one or more of the semicircles is seen.

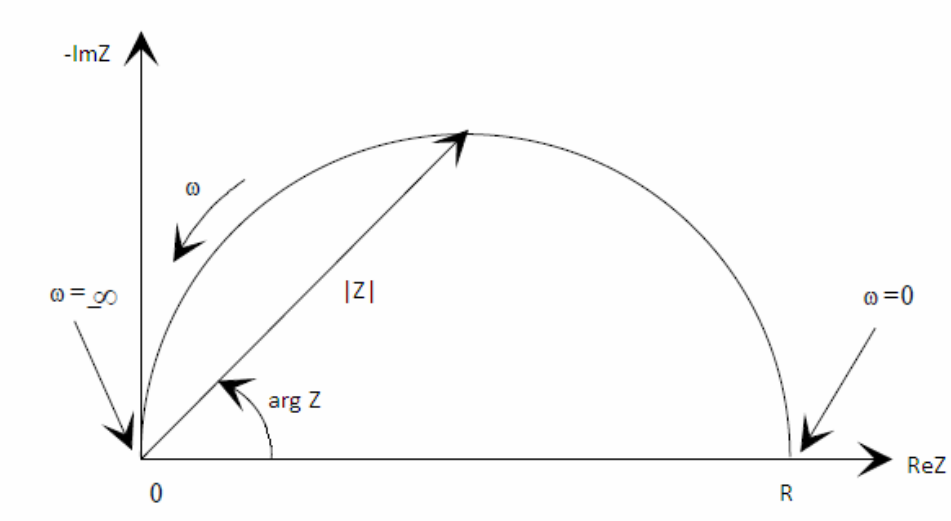


Figure 6. Nyquist plot with one time constant for the circuit shown in figure 7.

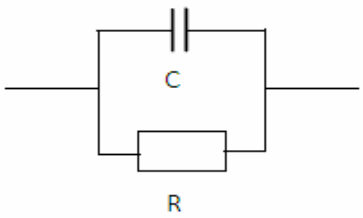


Figure 7. Simple circuit with one time constant.

Another way of expressing the impedance is the Bode plot. In Bode plot the impedance is plotted with log frequency on the x-axis and both the absolute value of the impedance ($|Z| = Z_0$) and phase-shift on the y-axis. The Bode plot for the electric circuit of Figure 7 is shown in Figure 8. Unlike the Nyquist plot, the Bode plot explicitly shows frequency information.

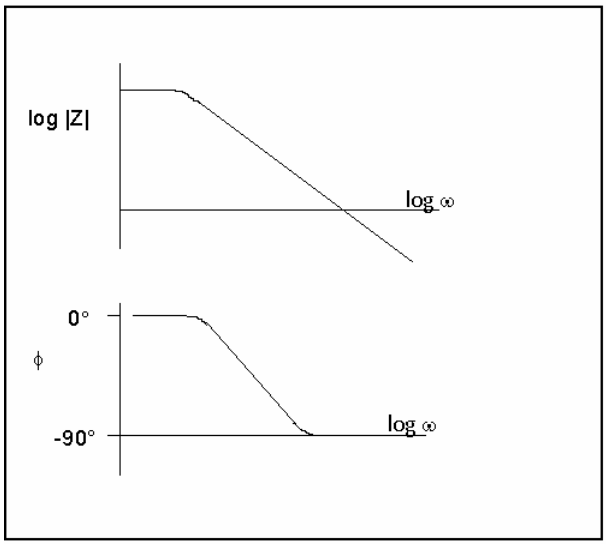


Figure 8. Bode plot with one time constant.

### 3.4.1 Corrosion rate from impedance plot

In a Nyquist plot as shown in figure 9, at very high frequency, the imaginary component, Z'' disappears, leaving only the solution resistance, $R_s$. At very low frequency, Z'' again disappears, leaving a sum of $R_s$ and the Faradaic reaction resistance or polarisation resistance, $R_p$. The corrosion rate can be calculated by using the Stern-Geary equation by assuming a reasonable value for the beta coefficients.

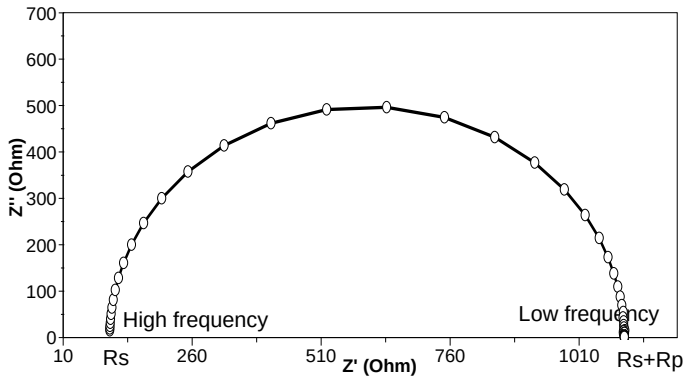


Figure 9. Nyquist plot showing the solution resistance and Polarization resistance.

In a bode plot the solution resistance and the polarization resistance can be read from the magnitude plot as shown in figure 10 and then can calculate the corrosion rate.

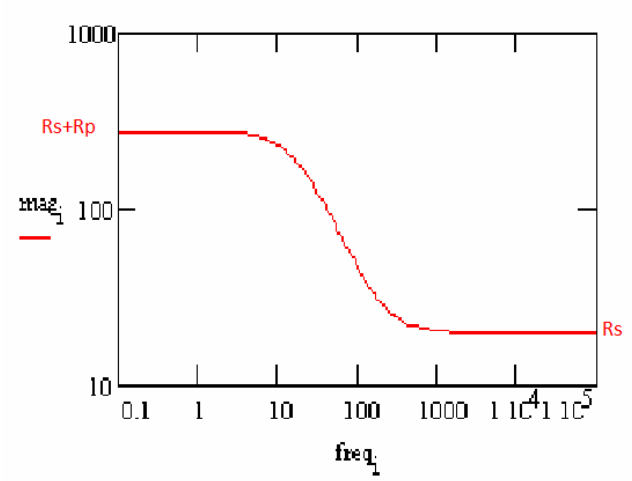


Figure 10. Bode plot showing solution resistance and Polarization resistance.

The various electrochemical methods described above is been referred from standard textbooks and research articles by various authors [17-19].

# 4. EXPERIMENTAL PROCEDURE AND SETUP

## Research objectives

The objective of this project is to study the corrosion behavior of carbon steel in the presence of both $CO_2$ and $H_2S$ in different pH and concentration. The test matrix for the research is given in Table 1

Table1. The Experimental test matrix

| | |
|---|---|
| Steel type | St 52-3 |
| Standard electrolyte | 0.5%NaCl |
| Temperature | 22˚C (room temperature) |
| pH | 3-10 |
| Concentration of sulfide | 1mM -50mM |
| Pressure | 1 bar |

Carbon steel is used for this purpose because it is one of the most widely used metal in the oil and gas industry. Table 2 shows the chemical composition of carbon steel (St 52-3), which was used for the research.

Table2. Chemical composition of Carbon Steel

| Element | Weight% |
|---|---|
| C | 0.15 |
| Si | 0.30 |
| Mn | 1.20 |
| P | 0.019 |
| S | 0.01 |
| Nb | 0.002 |
| Fe | 98.319 |

The experiment was done in a galvanic setup with two carbon steel electrodes in different electrolytic solution.

The sample was prepared by cutting a carbon steel rod having a surface area of 0.785$cm^2$ into an approximate length of 1cm. A wire was soldered to the sample and it was molded with epoxy resin. The reference electrode used was a Ag/AgCl (Ref201, Radiometer Analytical, France), which has a potential of 0.197V vs. the standard hydrogen electrode (SHE) [20]. The accuracy of the reference electrode was checked every time before the experiment, against the standard Ag/AgCl electrode, the difference was 3mV or less in all cases.

For the galvanic coupling two glass cells and a lid for each cell is made, and appropriate holes are drilled in the lid for the electrodes, for a bridge and for nitrogen purging. The cells are made air tight by applying grease between the cell and the lid. As the holes for the electrode and the bridge are marginally larger than needed, a Teflon tape is used to seal the holes air tight.

Of the two cells, one cell is added with 0.5M NaCl solution and it is maintained at pH 7 while on the other cell the condition is varied. The two cells are connected by a tube (bridge) and the solution is pumped into the tube to facilitate the flow of ions between the cells. To minimize contamination of the blank cell with sulfide, each end of the bridge is filled with cotton, so that the sulfide gets filtered off during the ionic transfer. Also, a thread is drawn all the way through the bridge in order to prevent the formation of air bubbles and assure good electrolytic contact. Both cells are purged with nitrogen to prevent oxidation. The galvanic corrosion effect is monitored for 20 hours for each experiment. After 20 hours the galvanic setup is disconnected and the LPR measurement is taken for the working electrode for 1 hour with platinum as the counter electrode. The potential range for the LPR measurements are from -0.02V to 0.02V. The potentiodynamic polarization scans is made with an initial voltage of -0.9V and a final voltage of -0.5 V with a scan rate of 0.15mV/s. For galvanic corrosion measurements the reference electrode is placed in the blank cell to prevent contamination of the electrode by sulfide. For LPR measurements and potentiodynamic scan the reference electrode was introduced in the cell with the working electrode in a syringe. This was to improve the contact, as the potentiodynamic scan gave poor results when the reference electrode was placed in the blank cell. The contamination in this case is minimized by introducing

some cotton in the tube connected to the syringe. Figure 11 and 12 shows the experimental setup in detail.

As the carbonate film formed under $CO_2$ environment need longer time to form than the sulfide film in $H_2S$ environment, the samples are stored in a container with saline water purged with $CO_2$. The samples are kept in this environment for 40days before the start of the first experiment. The temperature of the environment was 20$^oC$ for the first 20 days and the temperature was raised to 40$^oC$ for the next 20 days. The raise in temperature is to increase the film formation rate, as higher temperature enhances the rate of precipitation.

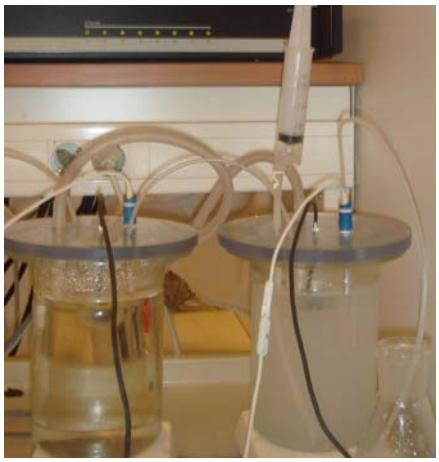

Figure 11. The Galvanic cell.

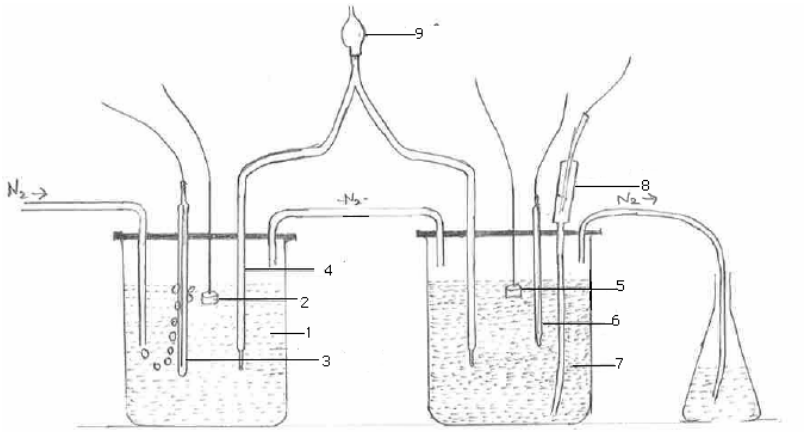


Figure 12. Diagram of the Galvanic cell- 1) 0.5M NaCl solution, 2) Counter electrode, 3) Reference electrode, 4) Bridge, 5) Working electrode, 6) Platinum electrode (for LPR measurement and Tafel scans), 7) The experimental solution, 8)Syringe (to insert reference electrode during LPR and Tafel scans), 9) Rubber bulb.

The experiments were performed with sodium sulfide as the source for $H_2S$ gas, as the use of $H_2S$ gas directly needs elaborate safety measures. Hence the amount of $H_2S$ produced depends on the pH of the solution. All the experiments are done with the Gamry Potentiostat. For galvanic measurement it was connected in zero resistance ammeter (ZRA) mode, which means metal 1 is connected as working electrode, metal 2 as the counter electrode and the reference to reference electrode The electrodes are polished with P120 silicon carbide paper before the start of each experiment. After each experiment an enlarged image of the working electrode is taken. The SEM imaging was also done to study the surface characteristics of the film. The SEM (Scanning Electron Microscope) EDX (Energy dispersive X-ray) analysis was done to find the elemental composition in the metal film. The accelerating voltage applied for SEM imaging was 10kV, in order to get a clear surface structure without damaging the surface film, as higher accelerating voltage gives high resolution but unclear surface structure and can damage the film.

The electrochemical impedance spectroscopy (EIS) analysis was done for the concentration of 10mM sulfide at pH 7 for a frequency range of 20,000 to 0.05Hz.

## 5. RESULTS AND DISCUSSION

The experimental results obtained are presented below based on the sulfide concentration and pH.

Experimental Series 1:

a. $H_2S$ Corrosion- pH= 3, Concentration of Sulfide= 1mM, 10mM, 50mM
b. $CO_2/H_2S$ Corrosion- pH= 3, Concentration of Sulfide= 1mM, 10mM, 50mM

Experimental Series 2:

a. $H_2S$ Corrosion- pH= 7, Concentration of Sulfide= 1mM, 10mM, 50mM
b. $CO_2/H_2S$ Corrosion- pH= 7, Concentration of Sulfide= 1mM, 10mM, 50mM

Experimental Series 3:

a. $H_2S$ corrosion- pH= 10, Concentration of Sulfide= 1mM, 10mM, 50mM
b. $CO_2/H_2S$ corrosion- pH= 10, Concentration of Sulfide= 1mM, 10mM, 50mM

Experimental Series 4:

a. $H_2S$ and $CO_2/H_2S$ corrosion -EIS Analysis, Concentration of Sulfide= 10mM, pH= 7

**Experimental series 1a**

The galvanic currents in experiments with various concentration of sulfide at pH 3 are shown in figure 13. The general corrosion rate was expected to be high at pH 3 and the presence of $H_2S$ is supposed to further increase the rate of corrosion. But, the results obtained in the galvanic coupling shows negative current which means that the working electrode ($H_2S$ environment) is more electronegative than the counter electrode. This could be because of the film formation and hence the metal getting passive. It was found that the open circuit potential (OCP) for the two surface was different, a higher OCP at the working electrode ($H_2S$ environment) and a lower OCP at the counter electrode (blank). In figure 13, it can be seen that for 30 minutes to 1 hour the current was positive, suggesting that the passivation is due to film formation. Figure 14 shows the galvanic potential, which is a mixed potential of the working electrode and counter electrode, measured for 20 hours. It can be seen that the potential gradually decreases to the more negative region, driving the anodic current towards the counter electrode.

Work done by Han J et al [21] with iron carbonate film shows that in a galvanic setup, under film forming condition the bare metal corrodes one or more orders of magnitude faster than the film protected area. The result obtained was in agreement with this research, showing a high level of protection of the working electrode in a galvanic coupling but when the coupling is removed the metal shows high degree of corrosion.

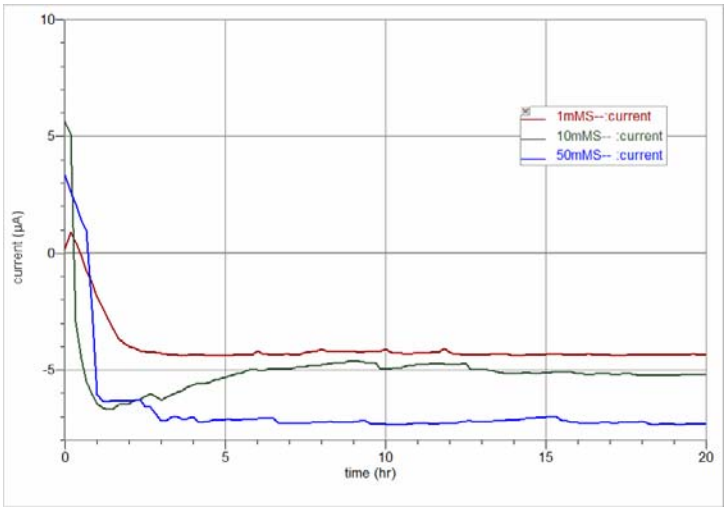


Figure 13. The change in galvanic current with time for concentration of sulfide at pH 3.

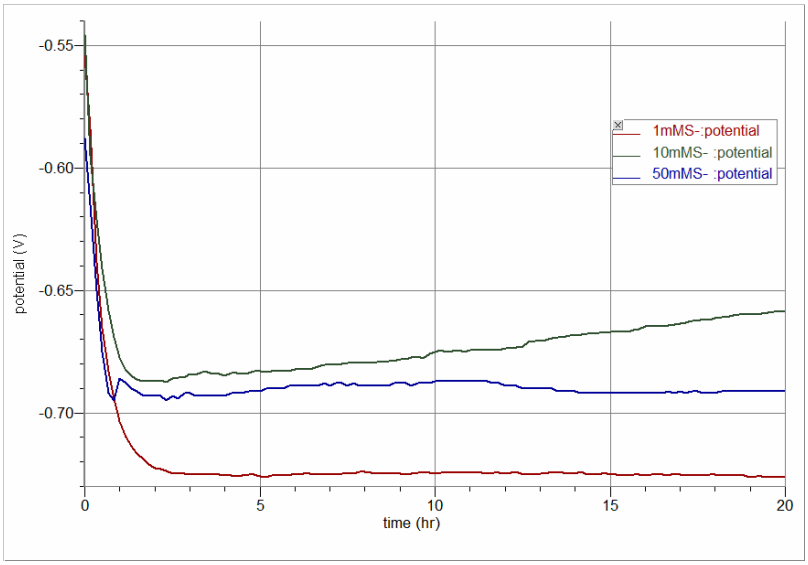


Figure 14. The galvanic potential versus time for various concentration of sulfide at pH 3.

Figure 15 shows the picture of the counter electrode taken after the end of the experiment with 50mM sulfide concentration. It shows that a uniform corrosion has occurred in the electrode. Figure 16 is the picture of the working electrode for the same experiment. It can be seen that the surface is covered with a thick black film. The corrosion rate of the two metal surfaces during the galvanic coupling was not measured, but the result suggests that the film covered surface is protected by the bare metal surface.

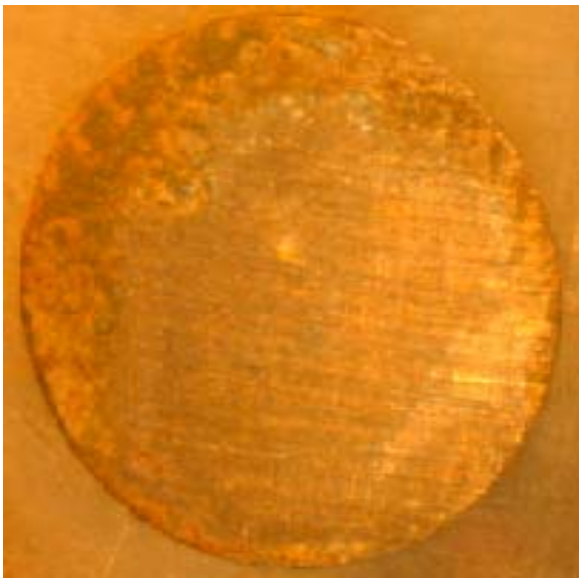

Figure 15 . Picture of the counter electrode for the experiment with a concentration of sulfide 50mM.

Figure 16. Picture of the working electrode for the experiment with a concentration of sulfide 50mM.

Figure 17 shows the potential measured with the various electrochemical techniques. Ec(Rp) and Ec(Tafel) are measured only for the working electrode after disconnecting the galvanic setup. At pH 3 as shown in figure 17 the galvanic potential was lower than the potential measured with LPR and Tafel. When compared with the potential-pH diagram (the Pourbaix diagram) for iron in figure 46 and 47, this potential is in the active region of corrosion.

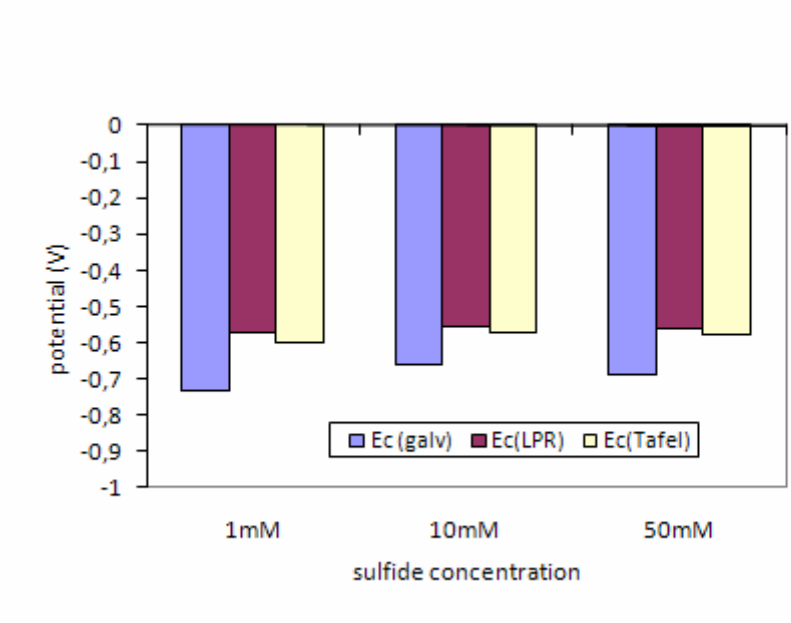


Figure 17. The change in potential at different concentration of sulfide at pH 3.

Figure 18 shows the potentiodynamic sweeps for various concentration of sulfide. It can be seen that at a higher concentration of sulfide (50mM) the corrosion current is increasing suggesting that, higher the concentration of sulfide more will be rate of corrosion. Figure 19 shows the corrosion rate calculated with LPR and Tafel. In general, the corrosion rate, calculated with LPR shows higher value than the rate measured with Tafel. But, the trend is the same for both types of measurement.

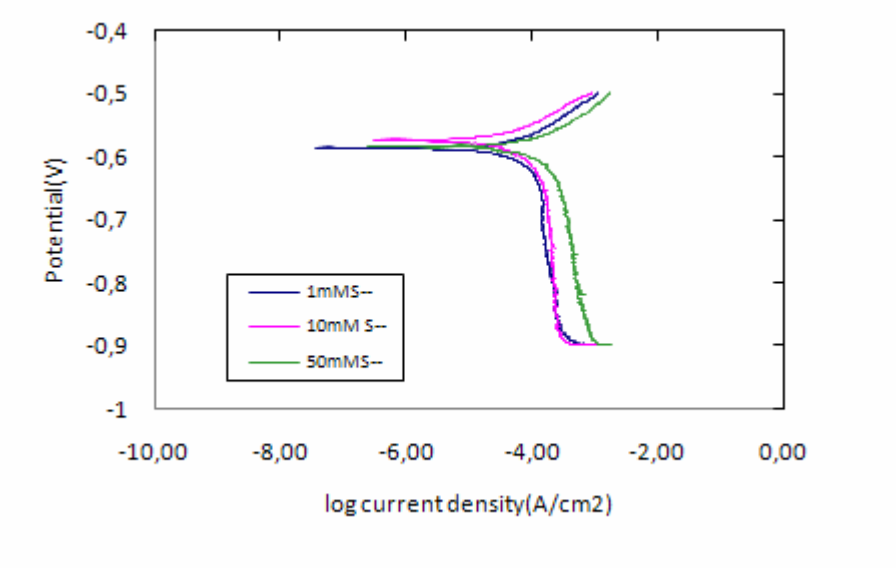


Figure 18. The potentiodynamic sweeps for various concentration of sulfide-1mM, 10mM, 50mM at pH 3 with bubbling $N_2$.

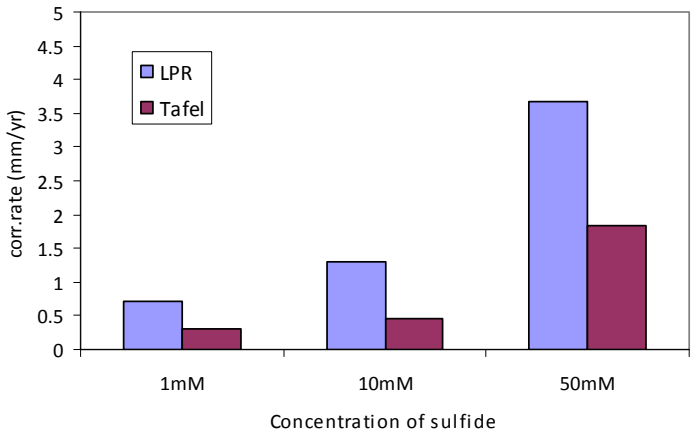


Figure 19. Effect of concentration on corrosion rate at pH 3 measured with LPR and Tafel.

**Experimental series 1b**

In this series, the experiments are done with the electrode pre-corroded with $CO_2$ for various concentration of sulfide at pH 3. The result obtained in this series is also similar to experimental series 1a. An important observation here is that the current (figure 20) was negative from the beginning of the experiment for all concentration of sulfides. This is because the electrode has an initial carbonate film when it was exposed to sulfide, so the electrode gets immediate protection and the bare metal starts corroding from the beginning. The potential (figure 21) measured with the

galvanic setup shows a gradual decrease in the potential, driving the corrosion current in the opposite direction. Figure 22 shows the potential measured by all three methods. It shows that the galvanic potential is lower than the potential measured by LPR and Tafel. When compared with the Pourbaix diagram (figure 46 and 47) this potential without the galvanic coupling measured by LPR and Tafel are well into the corrosion region.

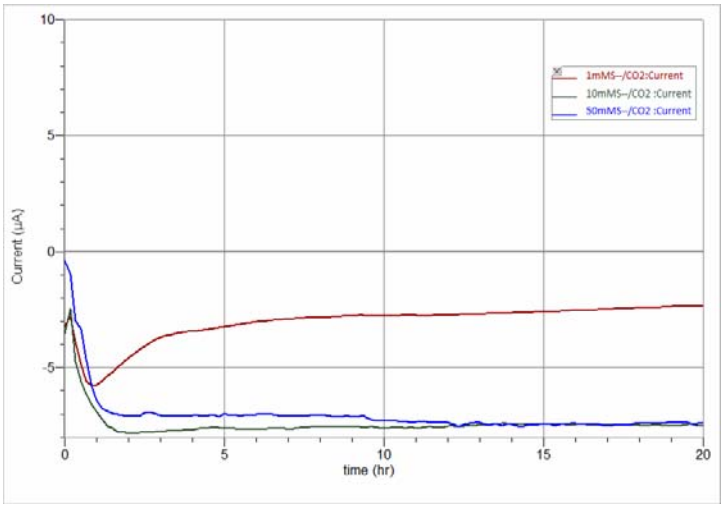


Figure 20. The galvanic current versus time at pH 3 for various concentration of sulfide in the presence of $CO_2$.

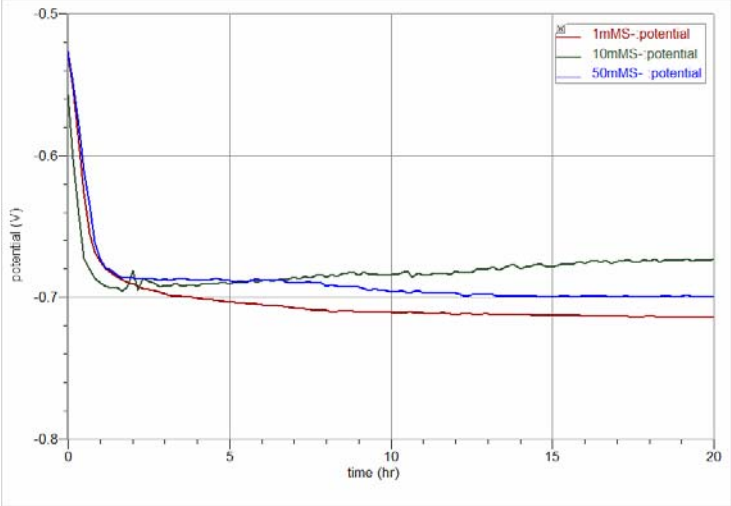


Figure 21. The galvanic potential versus time for various concentration of sulfide at pH 3 in the presence of $CO_2$.

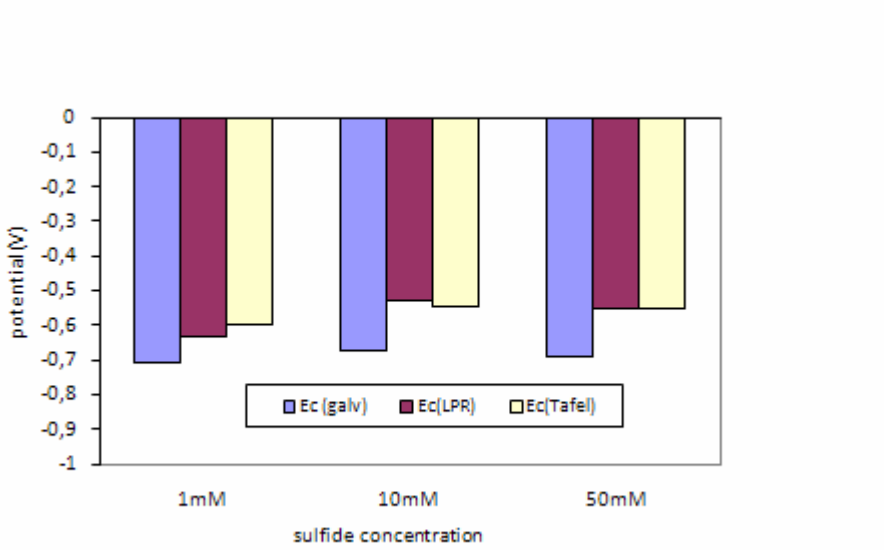


Figure 22. The change in potential at different concentration of sulfide at pH 3 in the presence of $CO_2$.

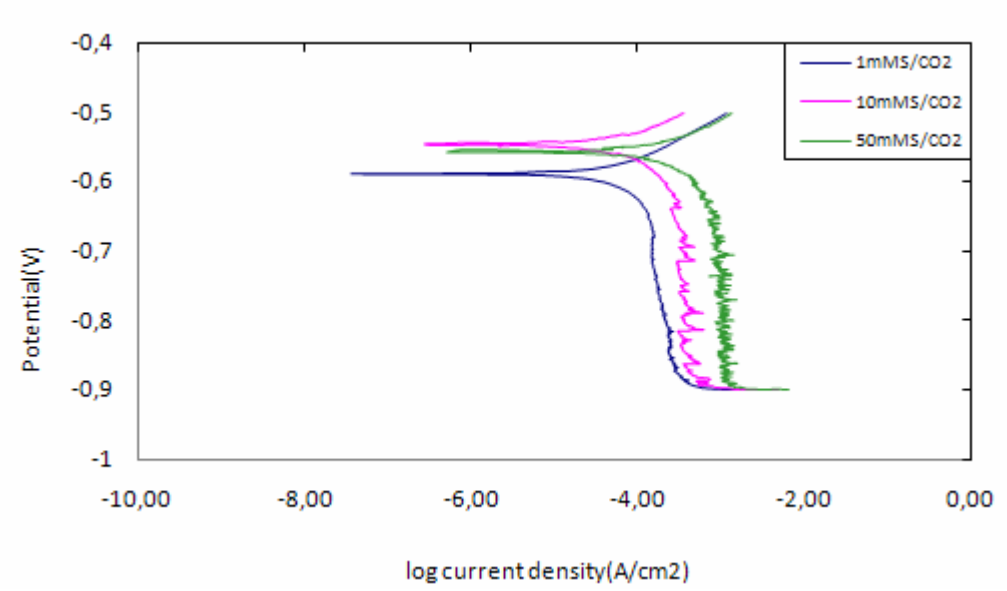


Figure 23. The potentiodynamic sweeps for various concentration of sulfide- 1mM, 10mM, 50mM at pH 3 with $N_2$ and $CO_2$.

Figure 23 shows the potentiodynamic sweep of the working electrode at different concentration of sulfide. It shows a gradual increase in corrosion current for increase in the concentration of the sulfide. Figure 24 shows the corrosion rate calculated with LPR and Tafel. The rate of corrosion in the presence of carbonate film is found to be more than the one without carbonate film. Most of the literature[10] suggest that the carbonate film forms a very strong protective layer and prevents corrosion. But, the result of this experiment was not in agreement with this theory.

According to some recent research [21-23], the passive carbonate film can be depassivated by decrease in pH. Also, the carbon dioxide gas is not supplied continuously into the experimental environment and this undersaturation could have dissolved the iron carbonate film. As the film dissolves, the irregular surface beneath the film provides more space for reaction and hence the corrosion rate is very high.

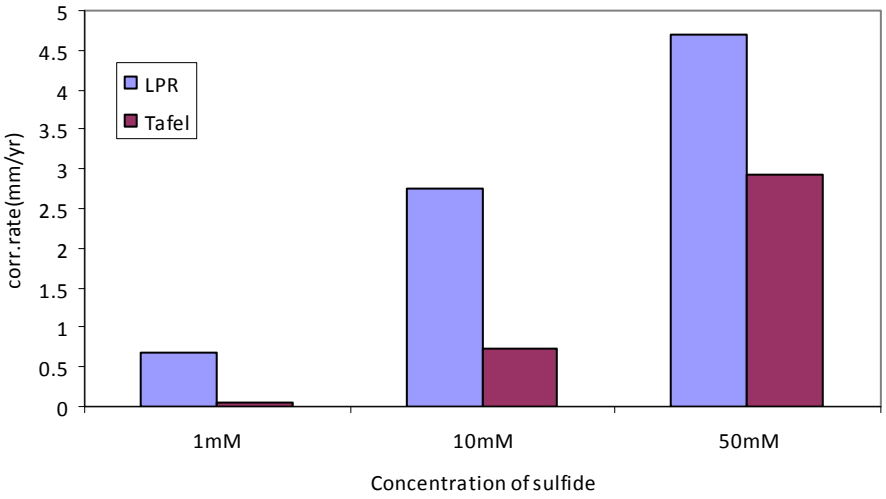


Figure 24. The effect of concentration on corrosion rate at pH 3 in the presence of $CO_2$.

**Experimental series 2a**

In this series of experiment the electrochemical measurements are taken at pH 7 for various concentration of sulfide. In the galvanic coupling, both the metals are immersed in solution with pH 7. The difference in environment is just by the sulfide concentration. The galvanic measurement shows negative current (figure 25) which means the counter electrode acts as anode. For at least 1 hour from the start of the experiment the current remains positive and then turn negative, suggesting the formation of film. The galvanic potential measurements (figure 26) show that the decrease in potential is driving the current in the opposite direction.

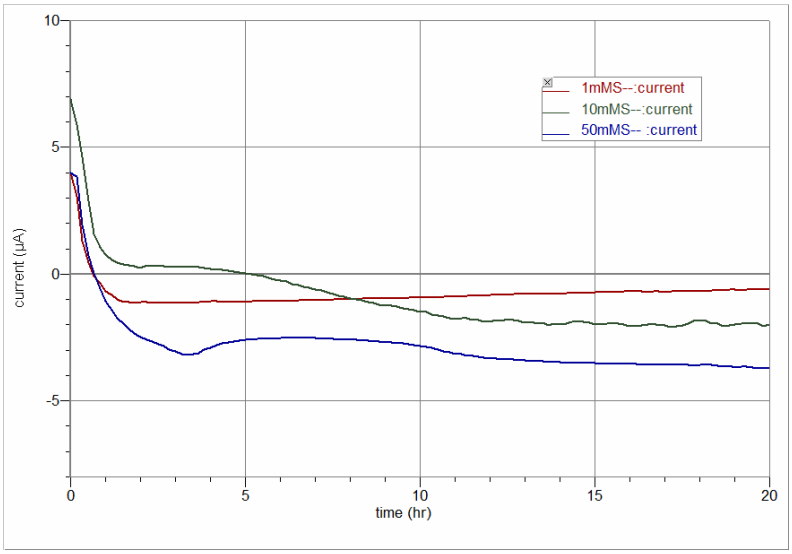


Figure 25. The change in galvanic current with time for the concentration of sulfide- 1mM, 10mM, 50mM at pH 7.

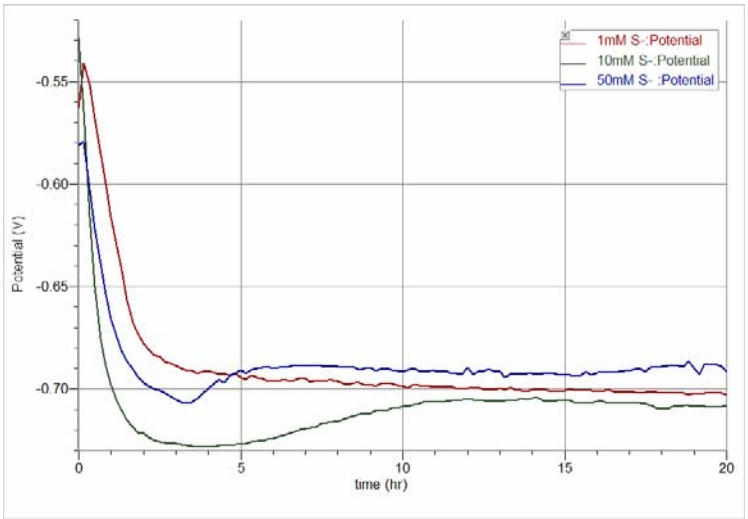


Figure 26. The galvanic potential versus time for various concentration of sulfide at pH 7.

The potential measured for the working electrode without the galvanic coupling by LPR and Tafel shows similar results as galvanic potential. In the pH range of 4 to 10, the corrosion rate of iron is relatively independent of the pH of the environment (figure 45). In this pH range the corrosion rate is governed largely by the rate at which oxygen reacts with absorbed atomic hydrogen, thereby depolarizing the

surface and allowing the reduction reaction to continue. As the experiment was done in presence of nitrogen the corrosion rate was very low for lower concentration of sulfide. At neutral pH, sodium sulfide produces very little $H_2S$, depending on the concentration of the sulfide. Also $Na_2S$ form a metal precipitate which is highly insoluble and prevents the metal from further attack. Thus, it can be seen that the rate of corrosion (figure 29) is fairly high for 50mM sulfide concentration (1.5 mm/yr) and for lower concentration the corrosion rate is negligible. The potentiodynamic scan (figure 28) also shows that higher concentration has higher degree of corrosion.

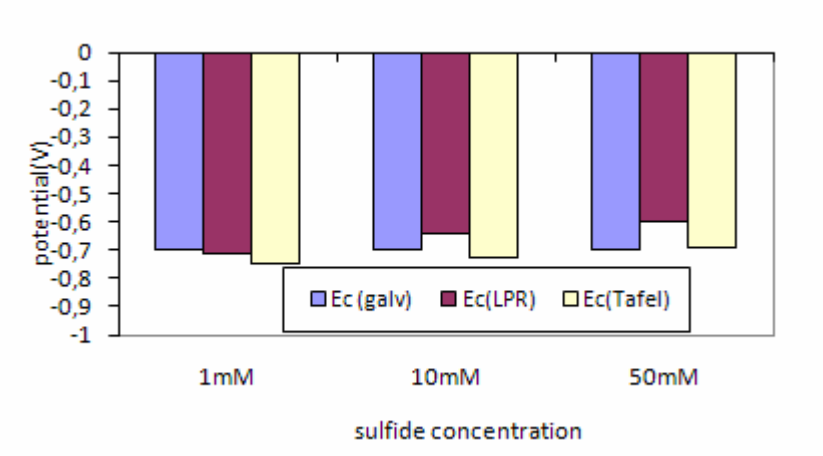


Figure 27. The change in potential at different concentration of sulfide at pH 7.

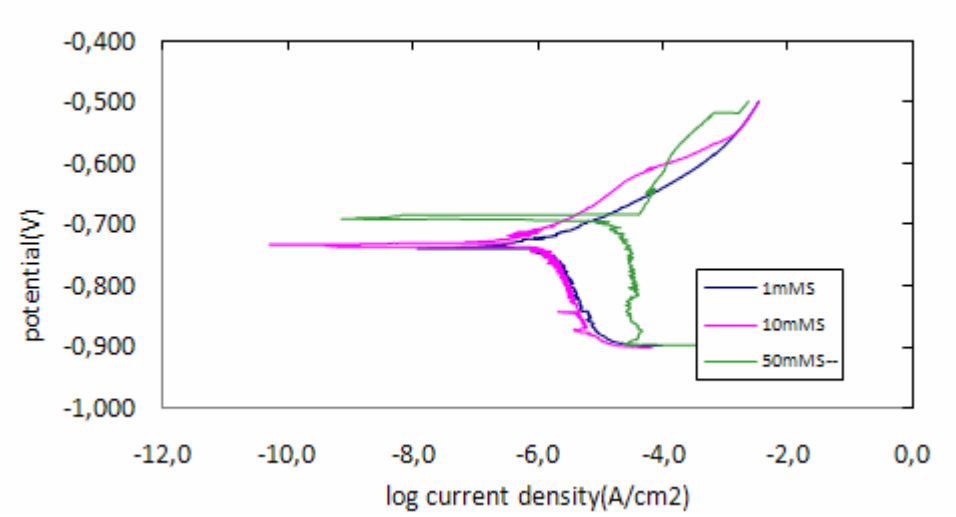


Figure 28. The potentiodynamic sweeps for various concentration of sulfide-1mM, 10mM, 50mM at pH 7 with bubbling $N_2$.

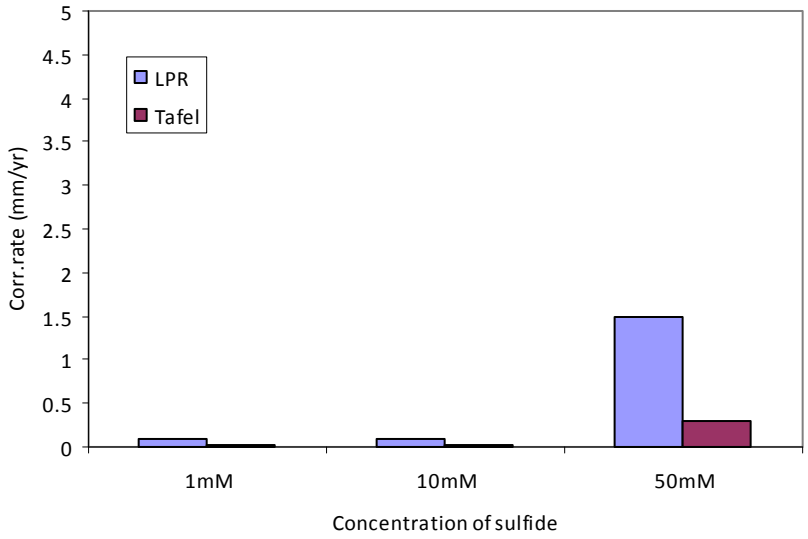


Figure 29. Corrosion rate at various concentration of sulfide at pH 7 measured with LPR and Tafel.

**Experimental series 2b**

In this series of experiment, the electrochemical measurement for the electrode covered with iron carbonate film is done for various concentration of sulfide at pH7. The galvanic current (figure 30) was negative as in the previous experiments. The galvanic potential (figure 31) decreases from the open circuit potential and stabilizing at a potential of around 0.710V, and gives cathodic current. The potential (figure 32) measured from LPR shows a higher potential than the galvanic, suggesting that the corrosion rate is low. As discussed in experimental series 2a, the neutral pH and oxygen free environment does not have much effect on corrosion. But, for higher concentration of sulfide it shows some corrosion effect (figure 34).

The potentiodynamic scan shows different potential for different concentration of sulfide (figure 33). This could be because of some minor changes in the environmental conditions.

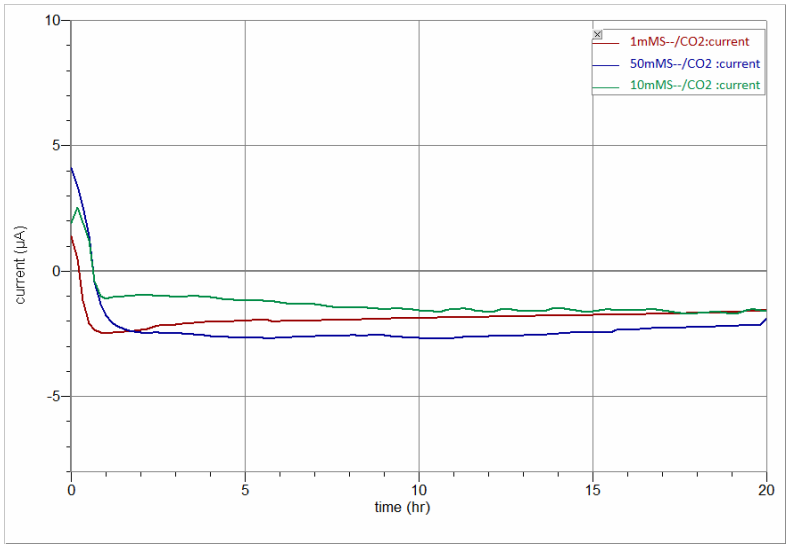


Figure 30. The galvanic current measured for 20 hours at pH 7 with concentration of sulfide as 1mM, 10mM, 50mM in the presence of $CO_2$.

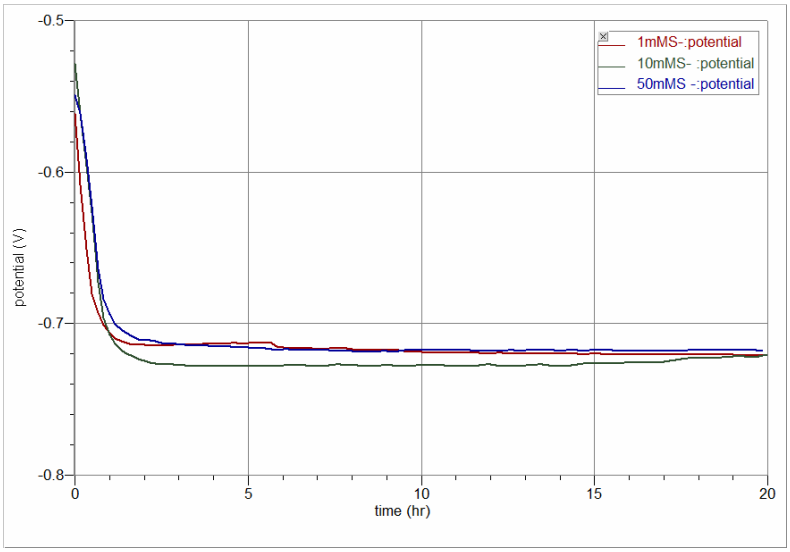


Figure 31. The galvanic potential versus time for various concentration of sulfide at pH 7 in the presence of $CO_2$.

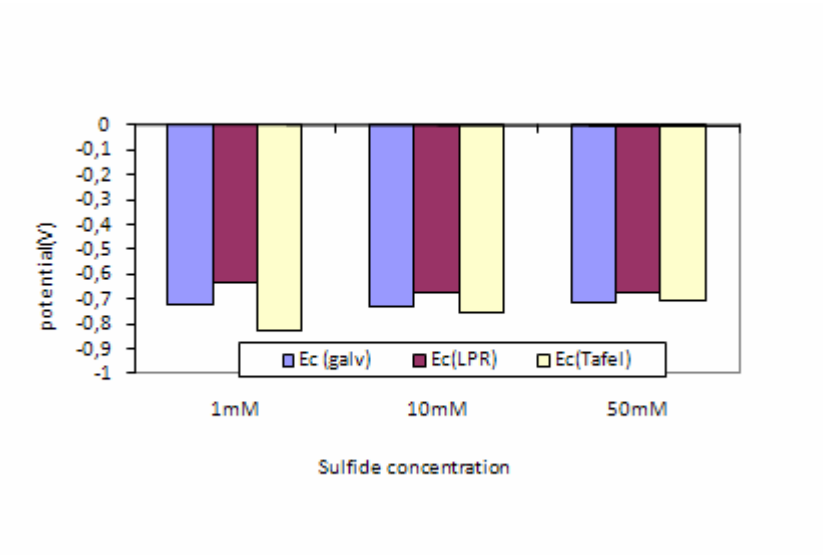


Figure 32. The change in potential at different concentration of sulfide at pH 7 in the presence of $CO_2$.

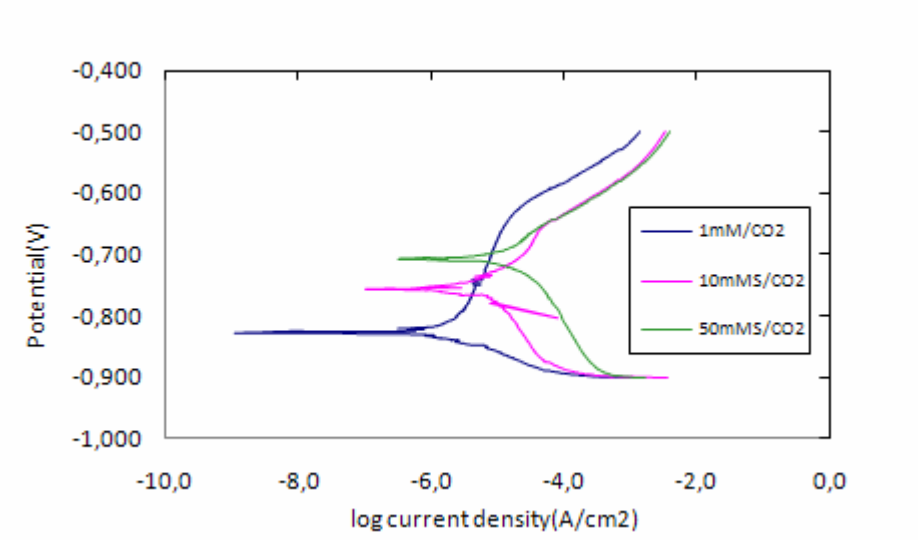


Figure 33. The potentiodynamic sweeps for various concentration of sulfide- 1mM, 10mM, 50mM at pH 7 with $N_2$ and $CO_2$.

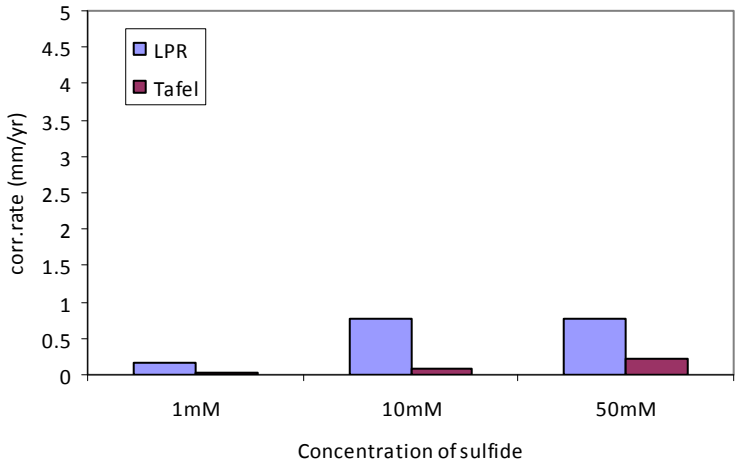


Figure 34. The corrosion rate measured with LPR and Tafel at various concentration of sulfide for pH 7 in the presence of $CO_2$.

**Experimental series 3a**

In this series of experiment the electrochemical measurement are taken at pH 10 for various concentration of sulfide. The galvanic corrosion current (figure 35) was almost zero, which means there is very little corrosion on both the metal surface. The OCP measured for the working electrode is lower than the counter electrode. So, the corrosion current is driving towards the working electrode, but at pH 10 this decrease in potential is in the region of immunity (figure 46 and 47). Hence, both the surface remains protected. Another reason for very little corrosion could be because of the use of sodium sulfide as the source of $H_2S$ gas. At higher pH sodium sulfide may not produce $H_2S$ gas and the dominant species could be $S^{2-}$, and the absence of $H^+$ ions decreases the corrosion rate. Also the reaction product, formed at higher pH is metal sulfides, which when precipitates on the surface of the metal gives protection to the metal as these metal precipitates have extremely low solubility [24]. It is also been observed by researches' that the film formation rate increases with pH while the corrosion rate decreases in electrolytes equilibrated in a hydrogen sulfide environment [25]. The general corrosion rate at pH 10 is also very low (figure 45). Even without the galvanic coupling, a very low corrosion rate was observed with LPR and polarization scan for all the concentration of sulfide measured. Hence, the sulfide concentration does not have an effect in causing corrosion at this pH. The potential (figure 37) measured with LPR and Tafel is very low. This might be because

of the formation of the passive film formed which lowers the potential. When this potential is compared with the Pourbaix diagram (figure 46 and 47), it is near to the region of immunity where no corrosion occurs. In fact, the corrosion rate measured with Tafel shows almost zero for all concentration of sulfides.

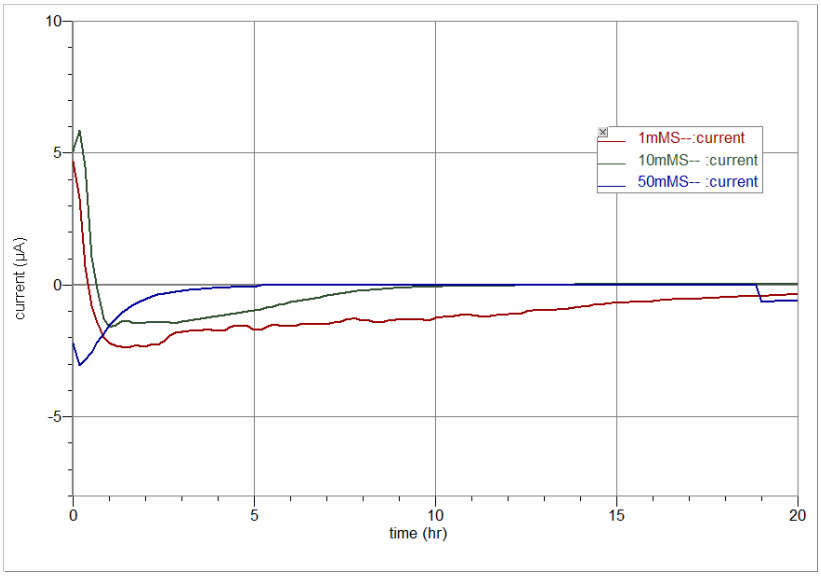


Figure 35. The galvanic current measured for 20 hours for the concentration of sulfide-1mM, 10mM, 50mM at pH 10.

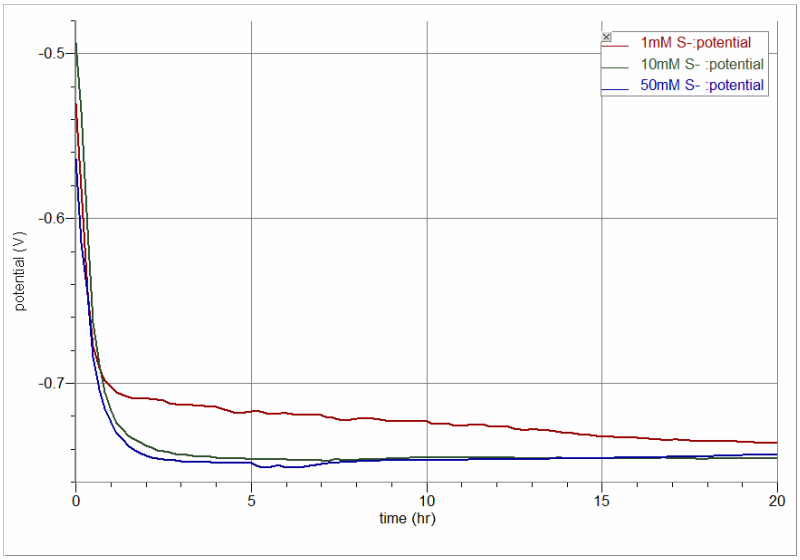


Figure 36. The galvanic potential versus time for various concentration of sulfide at pH10.

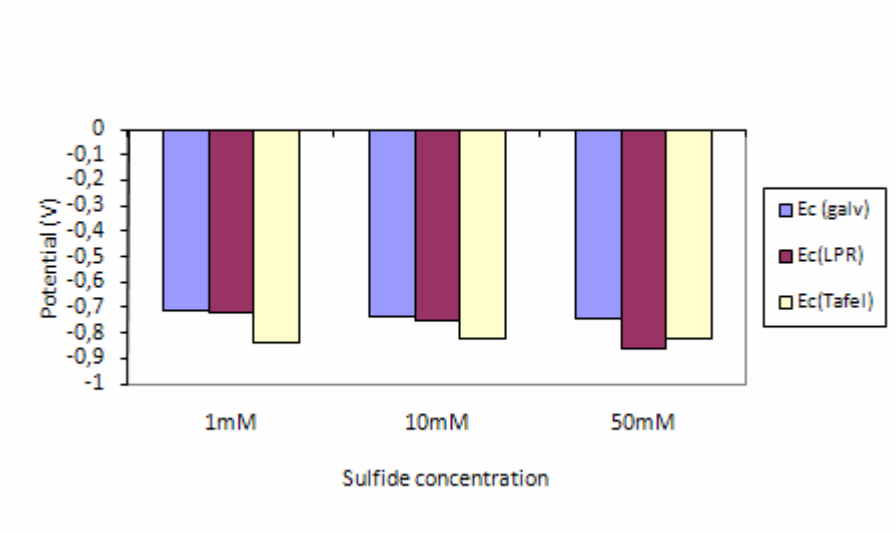


Figure 37. The change in potential at different concentration of sulfide at pH10.

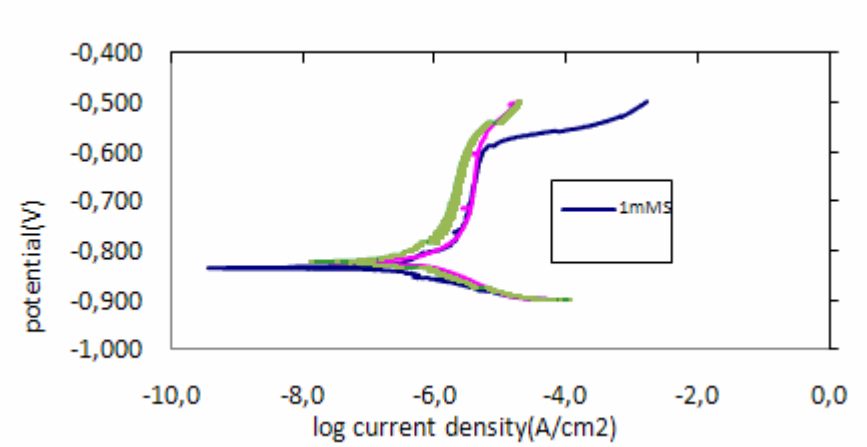


Figure 38. The potentiodynamic sweeps for various concentration of sulphide-1mM, 10mM, 50mM at pH 10 with bubbling $N_2$.

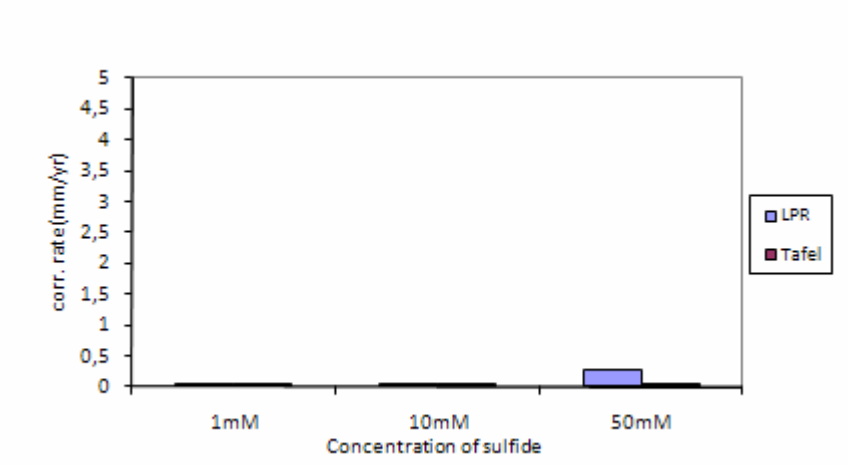


Figure 39. The corrosion rate measured with LPR and Tafel at pH10 for various concentration of sulfide.

**Experimental series 3b**

In this series of experiment the electrochemical measurements are taken for the electrode pre-corroded with $CO_2$ at pH 10. The galvanic current (figure 40) here shows positive, which means the working electrode (sulfide environment) is corroding. As discussed in experimental series 3a, the sulfide and its reaction product does not seem to increase the corrosion rate. But the results of galvanic current shows mild corrosion effect on the working electrode, it could be because of the difference in area between the two electrodes and also could be because of the presence of carbonate film. The pre-corroded metal surface has more area compared to the bare metal surface because of the irregularity of the surface. In the galvanic coupling the OCP measured for the working electrode was lower than the counter electrode. But, at pH 10 this potential was in the region of immunity (figure 46 and 47). So, it can be assumed that the corrosion effect in the working electrode could be because of the difference in area, which is making the working electrode as anode. The potential (figure 42) measured from all three methods were very low, suggesting that the probability of corrosion at this pH is negligible (from Pourbaix diagram figure 46 and 47). The corrosion rate (figure 44) measured with LPR shows around 1.5mm/yr for the concentration of 10mM sulfide and 50mM sulfide. This corrosion rate may not be due to the concentration of sulfide because 10mM sulfide shows slightly higher rate of corrosion than 50mM sulfide. This higher corrosion rate

than expected could be because of the irregular surface of the electrode. Also, the reaction product of sodium sulfide may have interfered with the carbonate film and might have caused a local condition near the metal surface, which enhances the corrosion rate.

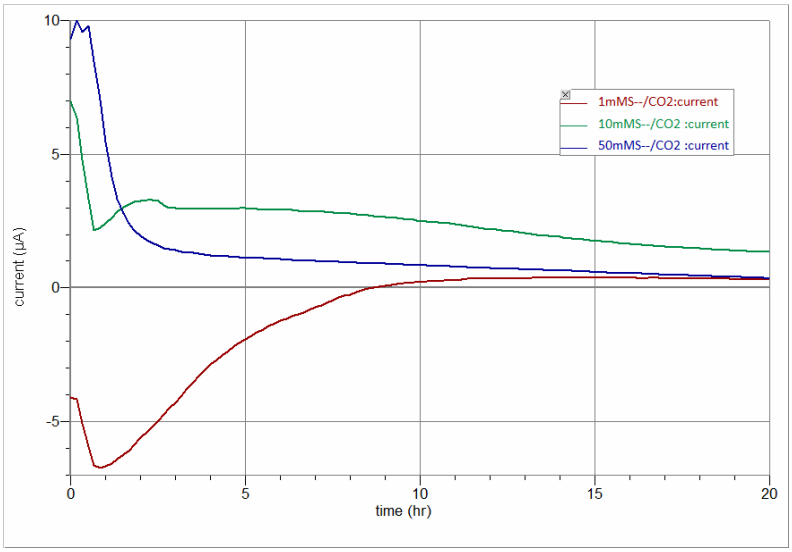


Figure 40. The galvanic current measured for 20 hours in the presence of $CO_2$ for various concentration of sulfide.

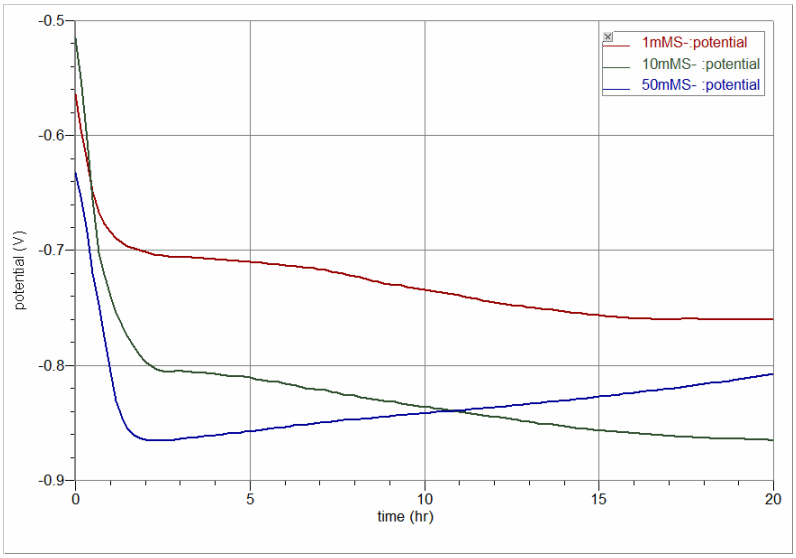


Figure 41. The galvanic potential versus time for various concentration of sulfide at pH 10 in the presence of $CO_2$.

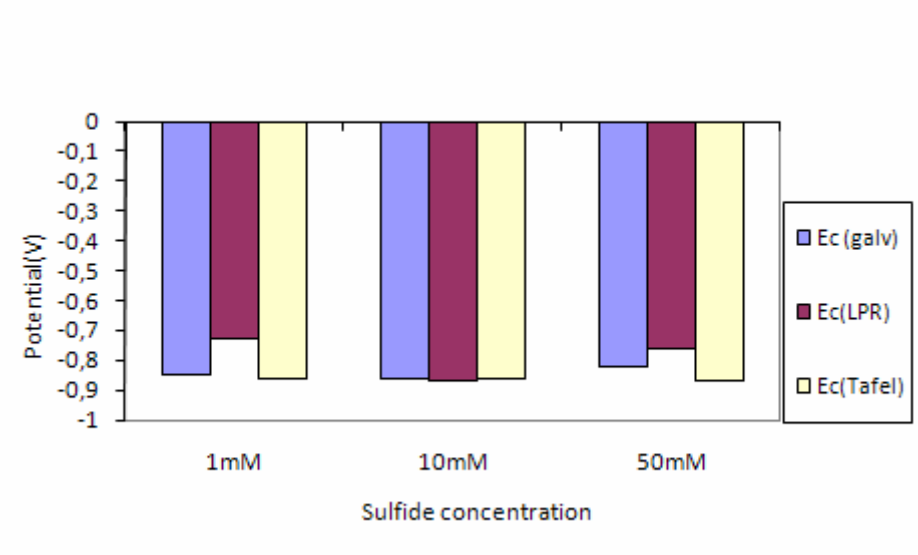


Figure 42. The change in potential at pH 10 for various concentration of sulfide in the presence of $CO_2$.

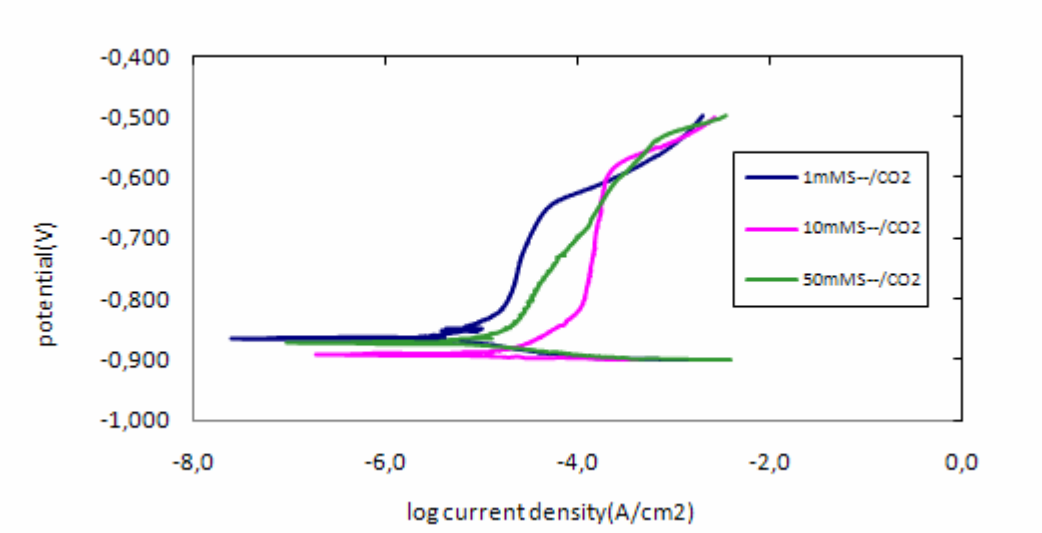


Figure 43. The potentiodynamic sweeps for various concentration of sulfide- 1mM, 10mM, 50mM at pH 10 with $N_2$ and $CO_2$.

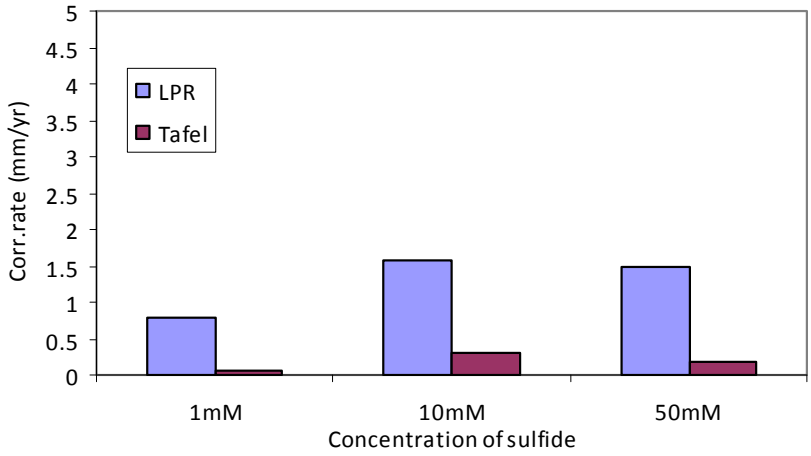


Figure 44. The corrosion rate measured with LPR and Tafel for various concentration of sulfide at pH 10 in the presence of $CO_2$.

**Standard results**

As the experiments are done by varying the pH of the solution it is necessary to analyze the results with a standard one. Figure 45 shows the general corrosion rate for different pH and figure 46, 47 are the Pourbaix diagram for iron in water at 25°C [16].

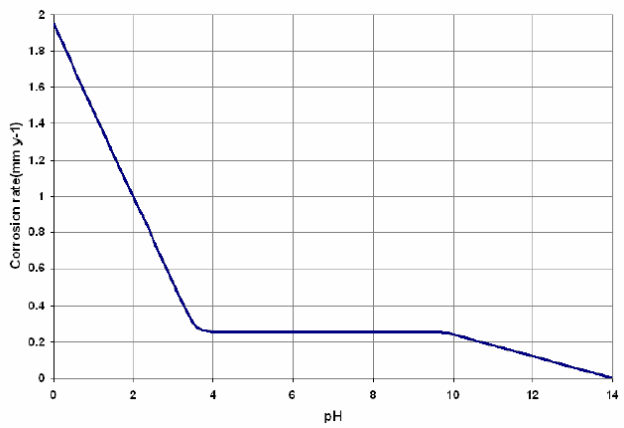


Figure 45. The effect of pH on general corrosion rate.

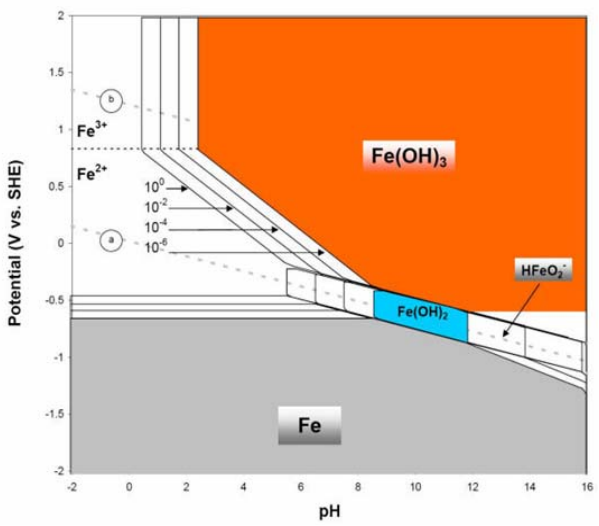


Figure 46. The potential-pH diagram for Iron in water at 25$^{o}$C

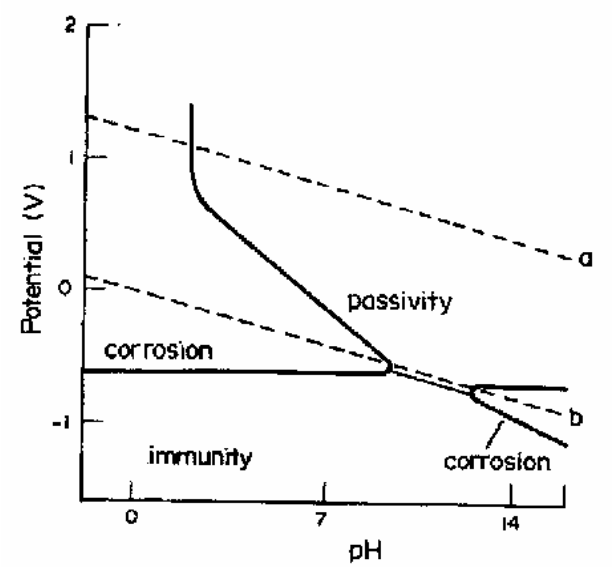


Figure 47. Theoretical conditions of corrosion, immunity and passivation of Iron.

**Results of Blank**

A set of experiment was done for pH 3, 7 and 10 without the addition of sulfide to compare the experimental results. Figure 48 shows the corrosion rate measured with Tafel and LPR. The LPR and the Tafel measurements for the working electrode are taken after 20 hours of galvanic coupling with the neutral solution.

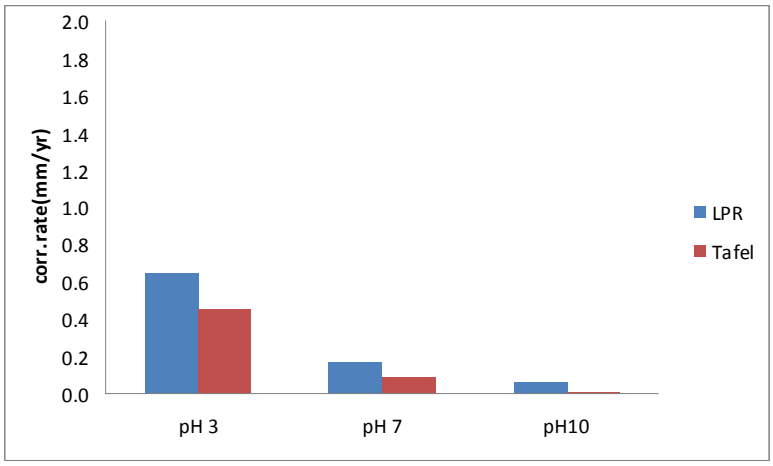


Figure 48. Corrosion rate measured for blank with LPR and Tafel.

**Experimental Series 4**

**EIS Analysis**

The EIS analysis was done as part of learning this technique to measure the corrosion rate. This technique was used to measure the corrosion rate for 10mM sulfide concentration at pH 7 with and without the presence of $CO_2$. The frequency range used for this technique was 20,000Hz to 0.05Hz. The Nyquist plot for the measurement with carbonate film is shown in figure 49. The measurement was taken initially in the presence of only $CO_2$ and $N_2$ and then after adding sodium sulfide. The lower frequency range is not small enough to determine exactly the point where the line crosses the intercept. Hence, the line is extrapolated to determine approximately the corrosion rate. The corrosion rate for the carbonate film covered surface before adding sodium sulfide was about 3mm/yr (the β coefficients was assumed to be 0.12V/decade for the corrosion rate calculation), which is very high at this pH. This suggest that the film formed has dissolved in the given environment and the irregular surface underneath was corroding at a higher rate. From figure 49 it can be seen that the corrosion rate tends to decrease after the addition of sodium sulfide. But as the data obtained was insufficient to calculate exactly the corrosion rate it can be assumed to be around 1mm/yr. In the previous experiments at pH 7, the corrosion rate was not measured during the start of the experiment, but the rate calculated after 20 hrs (figure 34) was 0.8mm/yr.

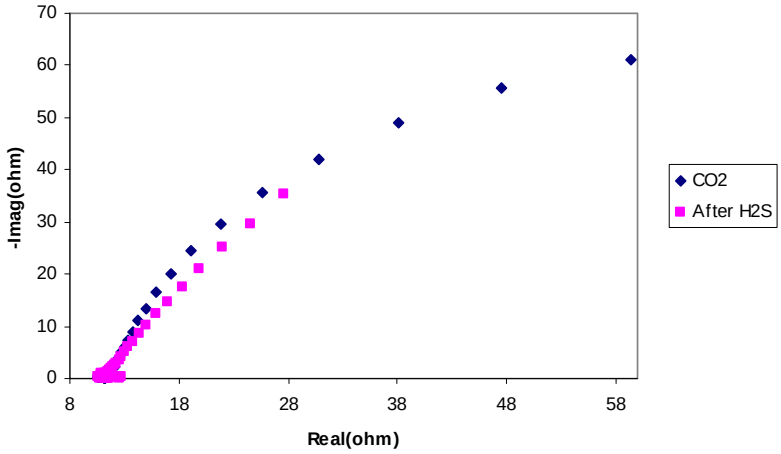


Figure 49. The Nyquist plot for $CO_2$ and $H_2S$ corrosion.

Figure 50 shows the Nyquist plot for 10mM sulfide concentration in the presence of nitrogen at pH7. Extrapolating the curve, the corrosion rate was calculated to be 0.86mm/yr, at the beginning of the experiment and this rate is reduced to about 0.54mm/yr after 20 hours. This suggests that the formation of the protective film is reducing the corrosion rate. Figure 51 and 52 shows the Bode plot for the same experiment. As there is very little data available in the low frequency region it is not possible to calculate the corrosion rate. Also, as the Bode plot cannot be extrapolated to get a reasonably accurate result.

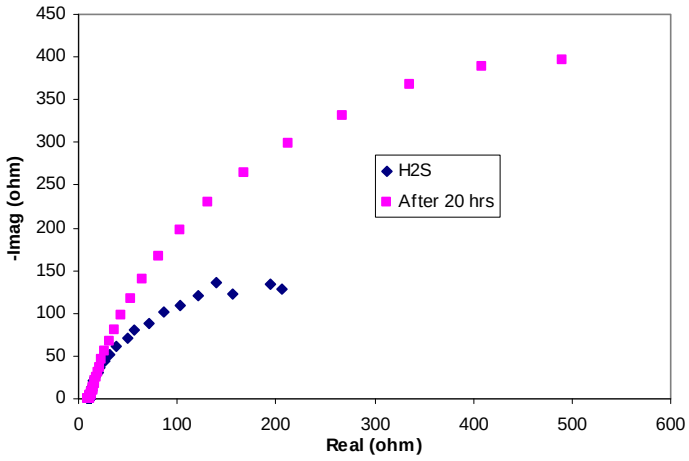


Figure 50. The Nyquist plot for $H_2S$ corrosion.

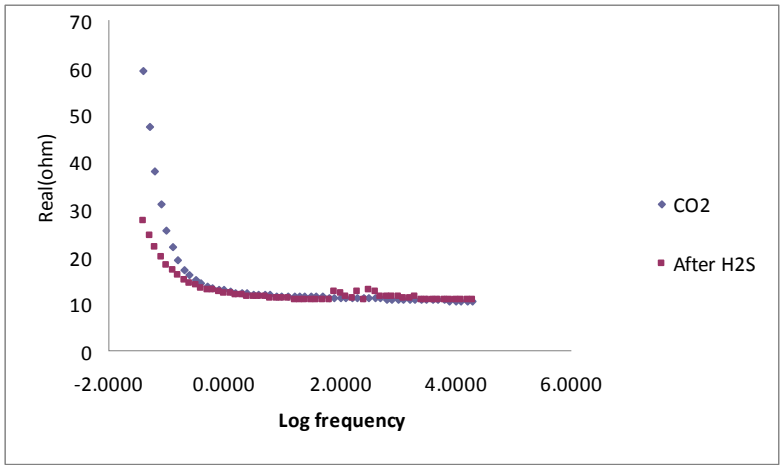


Figure 51. The Bode plot for $CO_2$ and $H_2S$ corrosion.

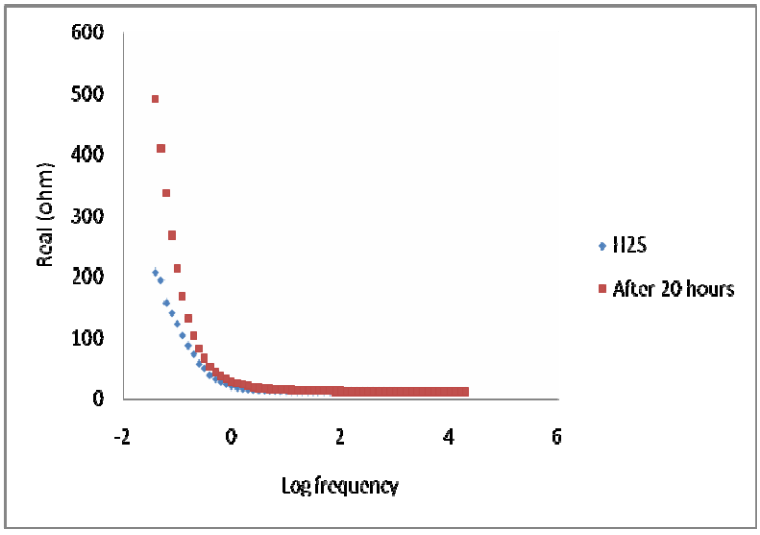


Figure 52. The Bode plot for $H_2S$ corrosion.

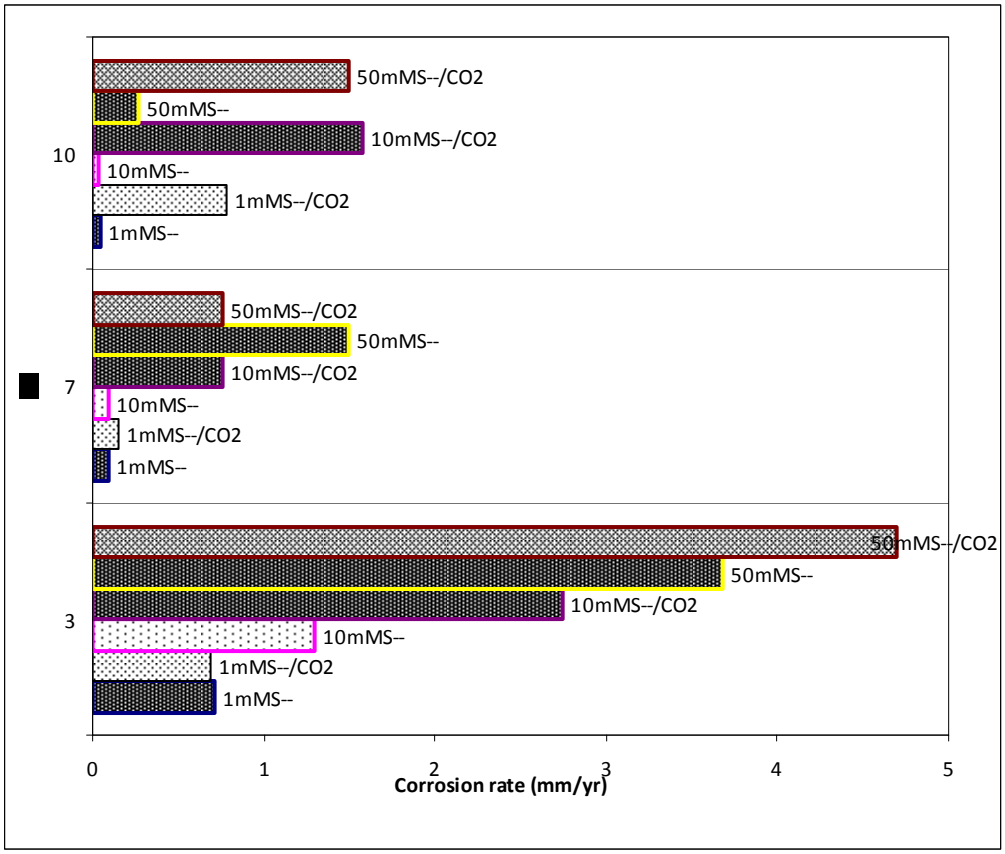


Figure 53. Summary of corrosion rate measured with LPR.

Table 3. Summary of corrosion rate.

| | Sulfide concentration | $H_2S$ system | | $CO_2/H_2S$ system | | Blank system | |
|---|---|---|---|---|---|---|---|
| | | LPR (mm/yr) | Tafel (mm/yr) | LPR (mm/yr) | Tafel (mm/yr) | LPR (mm/yr) | Tafel (mm/yr) |
| pH3 | 1mM | 0.711 | 0.294 | 0.685 | 0.045 | 0.650 | 0.450 |
| | 10mM | 1.293 | 0.454 | 2.743 | 0.736 | | |
| | 50mM | 3.683 | 1.846 | 4.699 | 2.933 | | |
| pH7 | 1mM | 0.091 | 0.023 | 0.152 | 0.029 | 0.170 | 0.090 |
| | 10mM | 0.096 | 0.023 | 0.762 | 0.091 | | |
| | 50mM | 1.498 | 0.292 | 0.762 | 0.222 | | |
| pH10 | 1mM | 0.050 | 0.002 | 0.787 | 0.073 | 0.058 | 0.005 |
| | 10mM | 0.040 | 0.005 | 1.575 | 0.292 | | |
| | 50mM | 0.271 | 0.018 | 1.498 | 0.182 | | |

Figure 53 shows the summary of corrosion rate measured with LPR at different pH levels for various concentration of sulfides. Table 3 summarizes the corrosion rate calculated with LPR and Tafel.

In general, it was found that the corrosion rate is high in the $CO_2$ /$H_2S$ system than it is with just $H_2S$. This could be because of the following reasons:

- For $CO_2$ /$H_2S$ corrosion the carbon dioxide gas is not supplied continuously in the experimental environment. The experiment was done on pre-corroded electrode with $CO_2$.
- The passivation due to iron carbonate film was lost when the metal was introduced in the $H_2S$ dominated system which has an undersaturation of carbon dioxide
- As the experiment was done on a pre-corroded electrode there is more surface available for $H_2S$ corrosion than the electrode which is not previously corroded with $CO_2$
- The experiment was done for a short period of time. The long term exposure could have given different result.
- The $H_2S$ gas is not added directly, it is added in the form of sodium sulfide.

**SEM Analysis**

The SEM analysis was done to study the surface characteristics of the film. Figure 54 shows the SEM image of the carbonate film. At higher magnification the film shows lots of cracks, which was not visible with naked eye. This crack is most probably caused due to the drying of the sample while imaging in the SEM. Figure 55 shows the SEM image of the film formed in the presence of both $CO_2$ and $H_2S$. The metal chosen for this imaging is the working electrode of the experiment with 50mM sulfide at pH 10. This electrode was chosen because the thickness of the film was maximum at pH 10. The surface topography of figure 54 is different from that of figure 55. The carbonate film (figure 54) is more rough or crystalline than the film formed in the presence of sulfide. In figure 54, images (c) and (d) are of almost the same magnification but the aperture size for (c) is 30 µm and for (d) is 60µm. The aperture size is increased to see more clearly the surface characteristics, as smaller aperture can give high depth of field but the resolution is not so good.

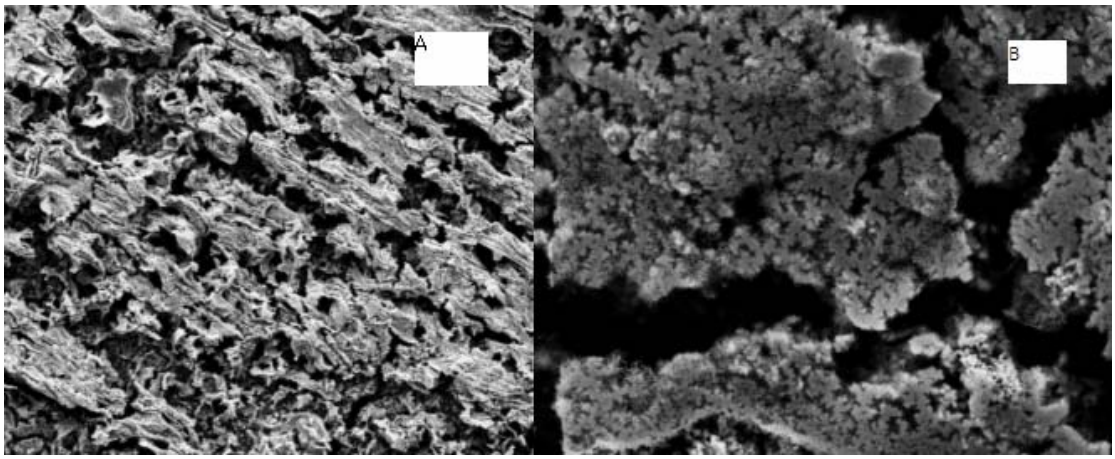


Figure54. SEM image of the electrode exposed to the solution purged with $CO_2$. Picture A is taken at a magnification of 400X and picture B at a magnification of 2000X

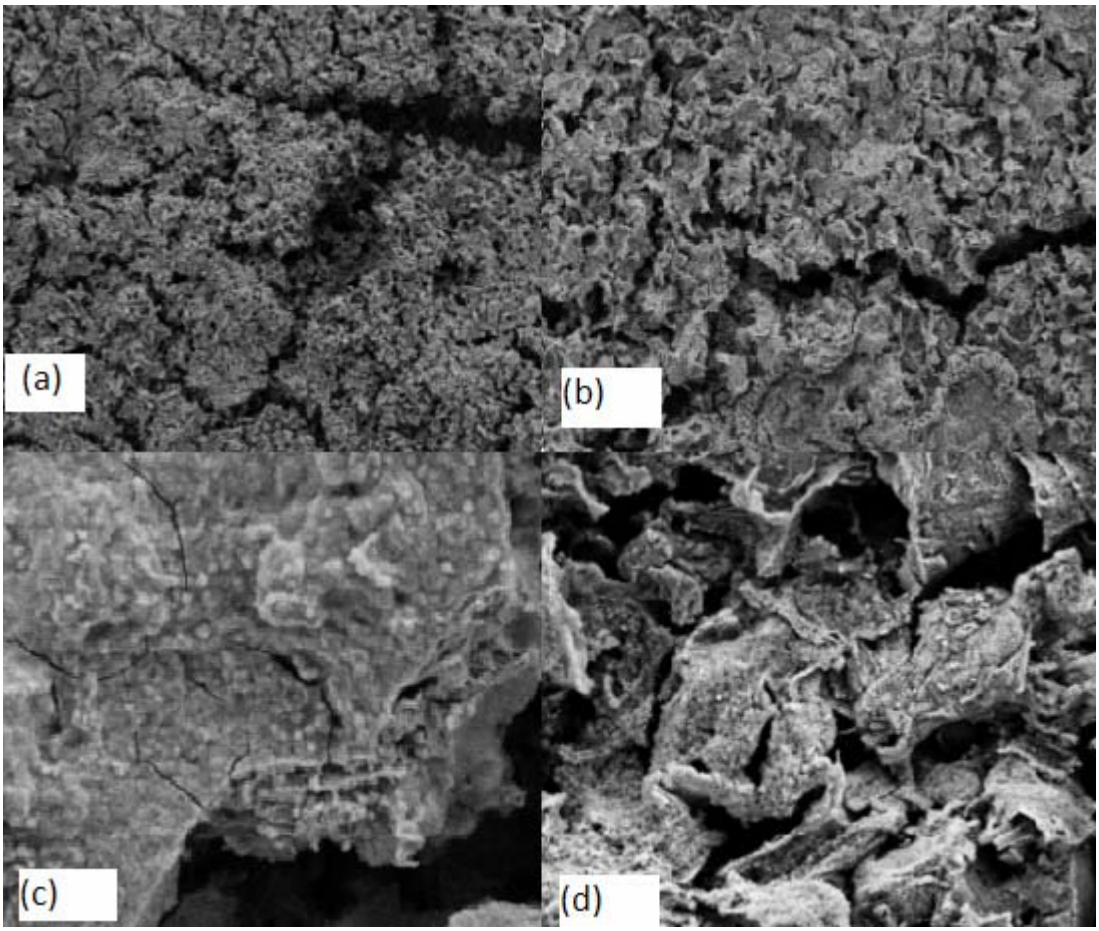


Figure55. The SEM pictures of the working electrode was taken for the experiment 50mM sulfide at pH10 in the presence of $CO_2$. The picture above shows the film at various magnification. a) 200X, b) 400X, c) 2030X, d) 2000X.

Figure 56 shows the cross section of the film at a magnification of 500X. The film formed was thick and the thickness of the film was approximately 100µm. Figure 57 shows the EDX analysis of the film done nearer to the surface of the metal and at the top of the film. It is found that at the surface of the film there was about 9% by weight of sulfur and at the bottom of the film it was 7.7%. This suggests that the carbonate film was more porous and the sulfide has penetrated through the film and attacked the metal surface. But, this result cannot be considered as accurate as sulfur is a low atomic weight species. The presence of silicon in the analysis is due to the polishing of the sample with silicon carbide paper

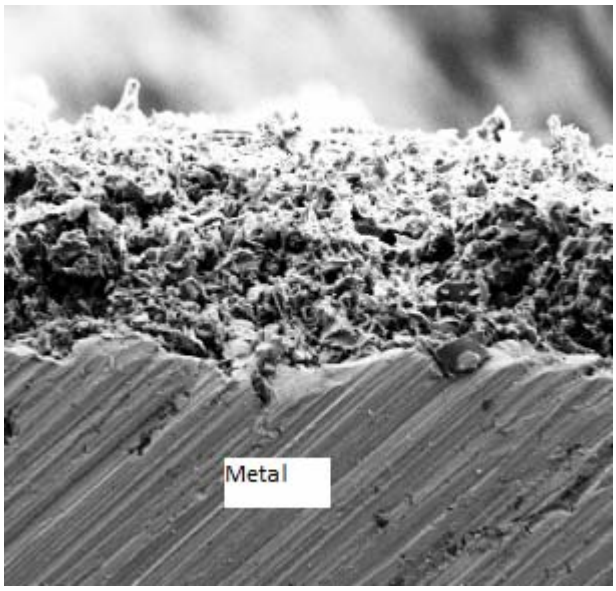


Figure56. SEM image of the cross-section of the film.

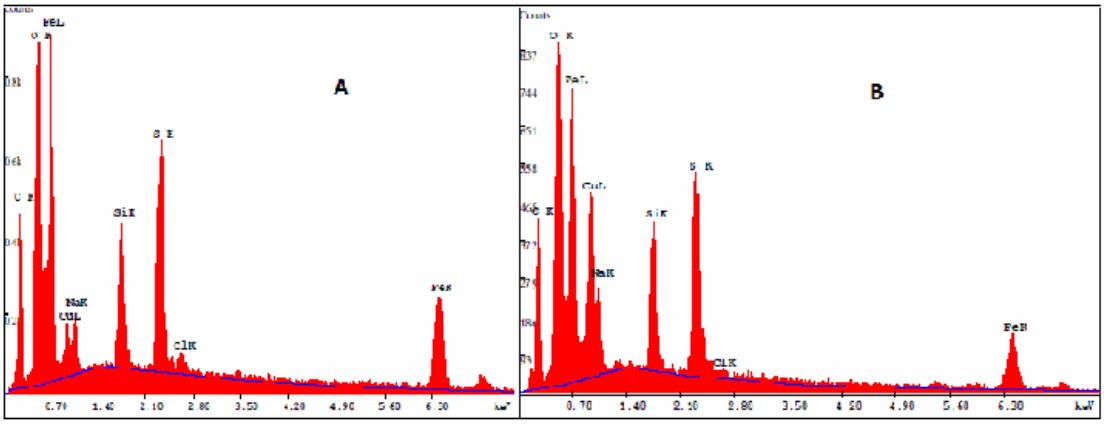


Figure57. The SEM X-ray analysis of cross section of the film. The picture A is taken near the metal surface (bottom of the film) and picture B on top of the film.

Figure 58 shows the surface analysis done on the surface of the film. This analysis was done at a magnification of 2000X. It was found that at the rough surface of the film the concentration of sulfide is about 15% by weight and at the smooth surface it was about 6% by weight, suggesting that the roughness of the surface is caused because of the sulfide film.

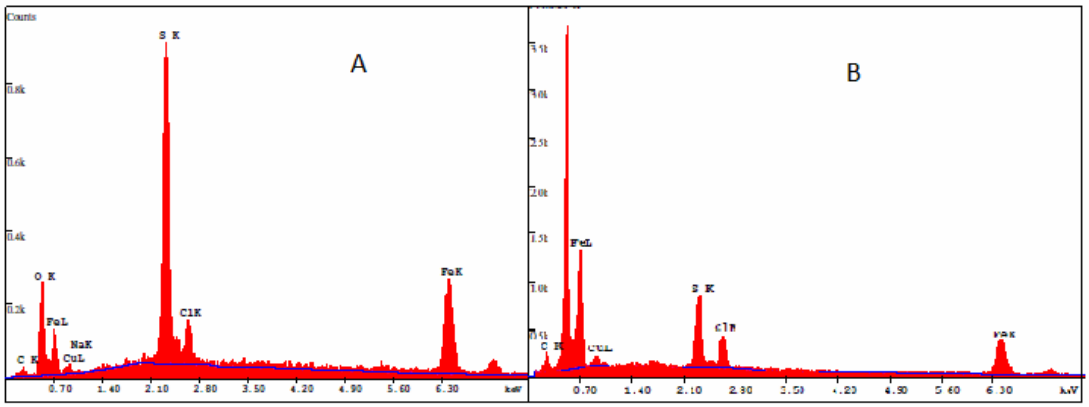


Figure58. The SEM EDX- analysis of the surface of the film. This analysis was done at a magnification of 2000X. Picture A is from a very rough surface of the film. PictureB is from a smooth surface of the film.

The EDX analysis for the composition of elements is given in detail in Appendix 2.

## 6. CONCLUSION

From the experiments performed on carbon steel (St 52-3) with galvanic coupling and without the coupling, the following conclusions can be made:

- In a galvanic coupling between metals, the metal exposed to even higher concentration of sulfide and lower pH gets protected and the bare metal which is in neutral pH was corroding.
- The corrosion rate in general was high for lower pH levels and higher concentration of sulfides.
- The corrosion rate is higher for the $CO_2$ /$H_2S$ system than in the presence of only $H_2S$.
- The Iron carbonate film formed appears to be a loose film if the concentration of the carbonate in the solution is not saturated. This condition is more observed at lower pH.

# 7. RECOMMENDATIONS AND FUTURE WORK

As this thesis is a short term project, many aspects related to the topic had to be overlooked because of the time limitation. The following could be some of the recommendations for future work

- Further study is needed on $CO_2$ and $H_2S$ corrosion for higher temperature and pressure, as the temperature and pressure are usually higher in oil and gas pipelines.
- All the experiments were done for a very limited period of 20-24 hours. A long term effect of the species on carbon steel can be investigated.
- Further study can be done by supplying $CO_2$ gas continuously into the experimental environment.

## 8. REFERENCES


1. Zhao G.X, et al., *'Formation Characteristic of CO2 Corrosion Product layer of P110 Steel Investigated by SEM and Electrochemical Technique'.* Iron and steel research International, Year 2009. **16**( 4): p. 89-94.
2. Hunnik E.W.J, V., Pots.B.F.M, and Hendriksen.E.L.J.A, *The Formation of Protective $FeCO_3$ Corrosion Product Layers in $CO_2$ Corrosion.* Corrosion/96, 1996(Paper No.6).
3. Gray L.G.S, et al., *Effect of pH and Temperature on the Mechanism of Carbon Steel Corrosion by Aqueous Carbon Dioxide.* Corrosion/90, 1990. **Paper No.40**(Houston, TX: NACE International, 1990).
4. Nesic S. and Lee K.L.J, *A Mechanistic Model of Iron Carbonate Film Growth and the Effect on $CO_2$ Corrosion of Mild Steel.* Corrosion/02, 2002. **Paper No. 237**.
5. Sun W and Nesic S, *A Mechanistic Model of $H_2S$ Corrosion of Mild Steel.* NACE Corrosion, 2007(Paper No.07655).
6. Sun W, Marquez A.I, and Botte G.G, *Theoretical Investigation of $H_2S$ Corrosion of Mild Steel.* Institiute of Corrosion and Multiphase Technology.
7. Ma H.Y, et al., *The influence of hydrogen sulfide on corrosion of iron under different conditions.* Corrosion Science, 1999(42): p. 1669-1683.
8. Shoesmith D.W, et al., *The Formation of Ferrous Monosulfide Polymorphs during the Corrosion of Iron by Aqueous Hydrogen Sulfide at $21^0C$.* Electrochemical Society, 1980. **127**(5): p. 1007-1015.
9. Rendon R.L and Alejandre J, *Molecular Dynamics Simulations of the Solubility of $H_2S$ and $CO_2$ in Water.* J.Mex.Chem.Soc2008. **52**(1): p. 88-92.
10. Hausler R.H and Godard H.P, *Advances in $CO_2$ Corrosion.* NACE Publication, 1984. **1**.
11. Srinivasan S and Kane R.D, *Prediction of Corrosivity of $CO_2/H_2S$ Production Environment.* Prevention of pipeline corrosion conference, Houston,TX, 1995.
12. Sun W and Nesic S, *Kinetics of Iron Sulfide and Mixed Iron Sulfide/Carbonate Scale Precipitation in $CO_2/H_2S$ Corrosion.* Corrosion NACExpo, 2006(Paper No.06644).
13. Wang H.B, et al., *Characterization of Inhibitor and Corrosion Product Film using Electrochemical Impedance Spectroscopy(EIS).* Corrosion 2001, 2001(Paper No.01023).
14. Nordsveen M, et al., *A Mechanistic Model for Carbon Dioxide Corrosion of Mild Steel in the Presence of Protective Iron Carbonate Films-Part 1: Theory and Verification.* Corrosion Science, 2003. **59**: p. 443-456.
15. Ma H.Y, et al., *Theoretical Interpretation on Impedance Spectra for Anodic Iron Dissolution in Acidic Solutions Containing Hydrogen Sulfide.* NACE Corrosion 1998. **54**(8).

16. Pourbaix M, *Atlas of Electrochemical Equilibria in Aqueous Solutions.* Nace International., 1966.
17. Enos D.G and Scribner L.L, *The Potentiodynamic Polarization Scan.* Technical Report 33, 1997.
18. Machiels A and Munson D, *Predictive Model for Galvanic Corrosion.* Electric power research institute, 2004.
19. Lasia A, *Electrochemical Impedance Spectroscopy and its Applications.* Kluwer Academic Publishers, 1999. **32**: p. 143-248.
20. Lundstrom M, Aromaa J, and Forsen O, *Redox potential characteristics of cupric chloride solutions.* Science Direct- Hydrometallurgy, 2008. **95**: p. 285-289.
21. Han J, et al., *Roles of Passivation and Galvanic Effects in Localized $CO_2$ Corrosion of Mild Steel.* Corrosion 2008, NACE International, 2008. **Paper No. 08332**.
22. Han J, et al., *Electrochemical Investigation of Localized $CO_2$ Corrosion on Mild Steel.* corrosion 2007, NACE International, 2007(paper No.07323).
23. Sun W, *Kinetics of Iron Carbonate and Iron Sulfide Scale Formation in $CO_2/H_2S$ Corrosion.* PhD dissertation, 2006.
24. David R.B, *Sodium Sulfides.* Kirk-Othmer Encyclopedia of Chemical Technology, 1997.
25. Hemmingsen T, Hilbert L, and Nielsen L.V, *Assessment of sulphur and $H_2S$ corrosion by use of simultaneous ER, galvanic and optical measurements.* Eurocorr 2003.

# Appendix 1

The result obtained for the galvanic coupling of metals was speculative, as the expected result was higher corrosion in the sulfide environment than for the metal in the neutral pH environment. In order to verify the authenticity of the results and to check whether the Zero Resistance Ammeter is connected in the correct direction in the Gamry potentiometer, a set of experiments was done for which the results are known.

**Galvanic coupling between carbon steel and duplex steel**

A galvanic coupling was made between carbon steel and duplex steel with the same experimental setup and neutral pH. The carbon steel was made the working electrode (metal 1) and the duplex steel as the counter electrode (metal 2). Figure 1 shows the galvanic current measured for 20 hours. As expected the current was positive and it is fairly high, suggesting that the carbon steel is corroding.

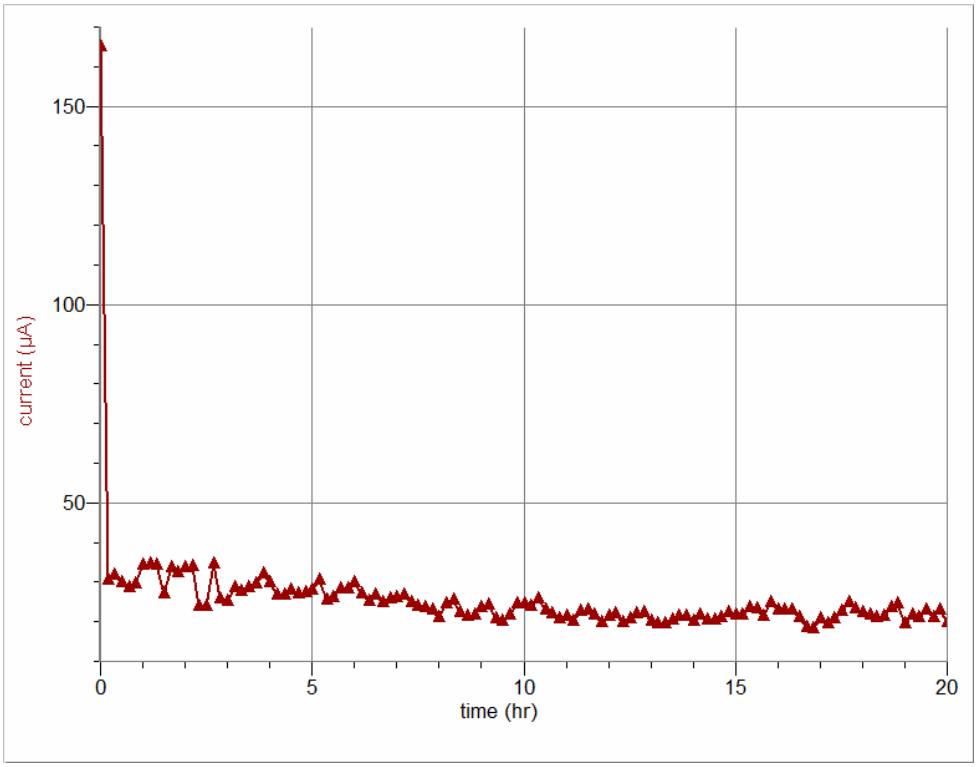


Figure 1. The galvanic current measured for carbon steel versus duplex steel.

Figure 2 shows the galvanic potential measured for 20 hours between carbon steel and duplex steel. The open circuit potential measured for carbon steel is lower than the duplex steel and hence the carbon steel acts as anode and the duplex steel as cathode. The potential measured is fairly constant for 20 hours.

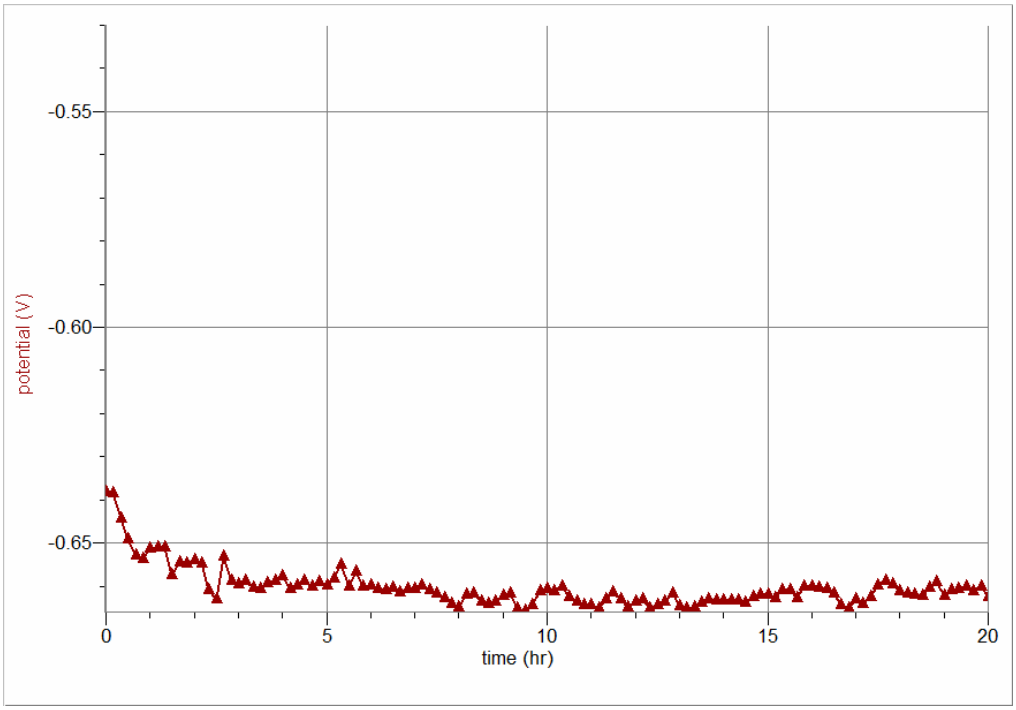


Figure 2. The galvanic potential measured for carbon steel vs. duplex steel.

# Appendix 2

### The SEM- EDX Analysis

The SEM- EDX analysis is done to study the surface characteristics of the film. Figure 3 and 4 give a clear picture of the elemental composition of the cross section of the film.

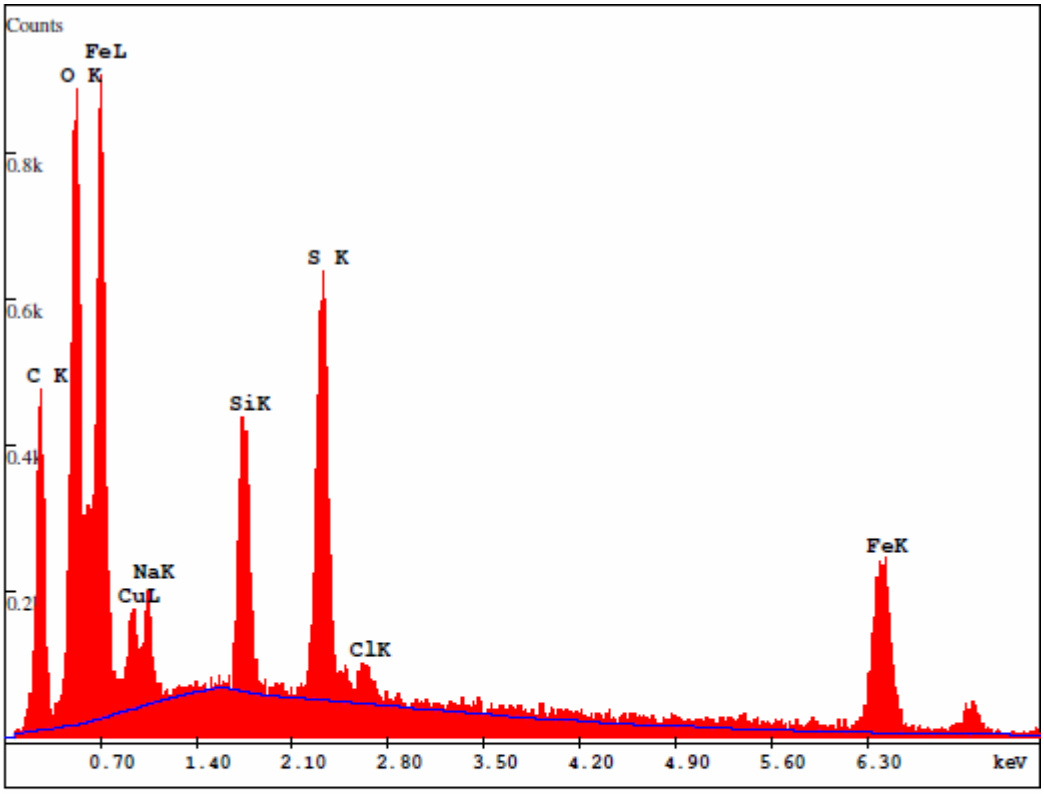


EDAX ZAF Quantification (Standardless)
Element Normalized
SEC Table : User c:\edax32\eds\genuser.sec

| Element | Wt % | At % | K-Ratio | Z | A | F |
|---|---|---|---|---|---|---|
| C K | 7.83 | 20.15 | 0.0189 | 1.1554 | 0.2091 | 1.0003 |
| O K | 15.89 | 30.70 | 0.0896 | 1.1284 | 0.4986 | 1.0018 |
| CuL | 4.02 | 1.96 | 0.0138 | 0.9004 | 0.3819 | 1.0003 |
| NaK | 1.82 | 2.44 | 0.0072 | 1.0555 | 0.3757 | 1.0003 |
| SiK | 4.17 | 4.59 | 0.0334 | 1.0675 | 0.7482 | 1.0016 |
| S K | 7.76 | 7.48 | 0.0714 | 1.0520 | 0.8745 | 1.0011 |
| ClK | 0.90 | 0.79 | 0.0081 | 1.0042 | 0.8946 | 1.0013 |
| FeK | 57.60 | 31.88 | 0.5287 | 0.9167 | 1.0003 | 1.0010 |
| Total | 100.00 | 100.00 | | | | |

Figure 3. The SEM- EDX analysis of the cross-section of the film. This analysis is done at the bottom of the film i.e., near the metal surface.

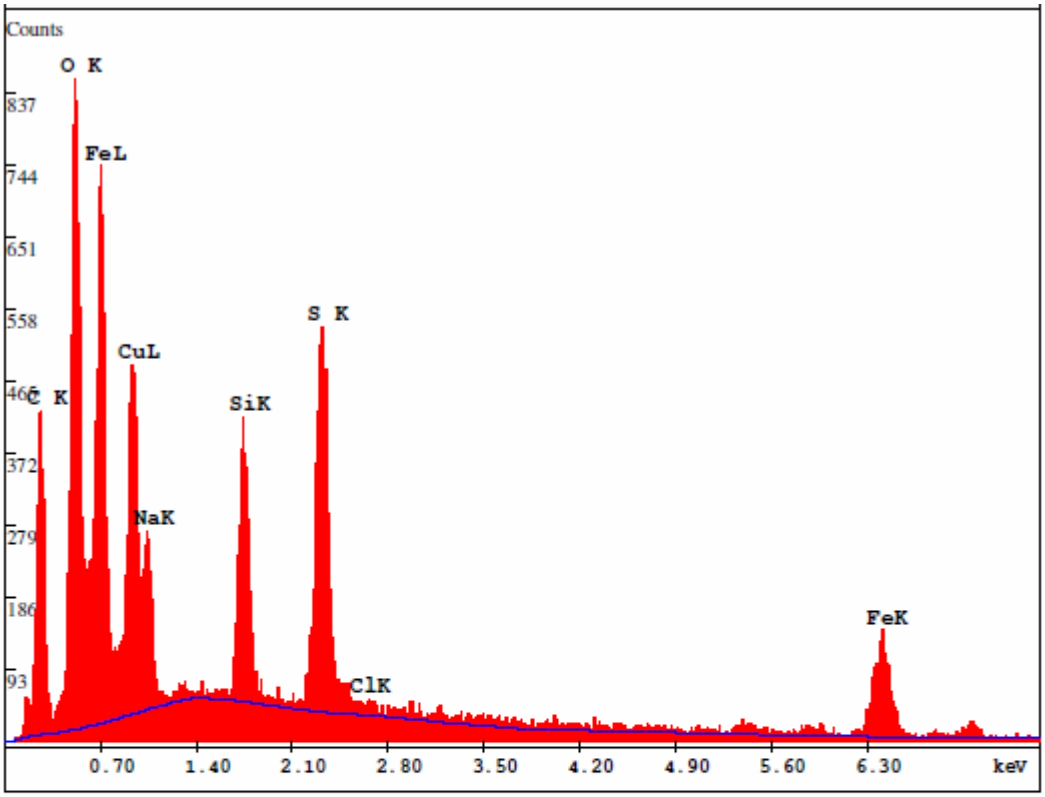


**EDAX ZAF Quantification (Standardless)**
**Element Normalized**
**SEC Table : User c:\edax32\eds\genuser.sec**

| Element | Wt % | At % | K-Ratio | Z | A | F |
|---|---|---|---|---|---|---|
| C K | 9.43 | 21.92 | 0.0220 | 1.1390 | 0.2048 | 1.0003 |
| O K | 20.23 | 35.31 | 0.1089 | 1.1126 | 0.4832 | 1.0012 |
| CuL | 14.24 | 6.26 | 0.0593 | 0.8880 | 0.4687 | 1.0004 |
| NaK | 3.77 | 4.58 | 0.0156 | 1.0395 | 0.3991 | 1.0004 |
| SiK | 4.75 | 4.73 | 0.0378 | 1.0519 | 0.7539 | 1.0017 |
| S K | 8.92 | 7.77 | 0.0811 | 1.0368 | 0.8760 | 1.0006 |
| ClK | 0.38 | 0.30 | 0.0034 | 0.9895 | 0.8923 | 1.0009 |
| FeK | 38.27 | 19.14 | 0.3467 | 0.9014 | 1.0003 | 1.0045 |
| Total | 100.00 | 100.00 | | | | |

Figure 4. The SEM- EDX analysis of the cross-section of the film. This analysis is done at the top of the film surface.

Figure 5 and 6 shows the SEM-EDX analysis of the surface of the film. Figure 5 shows the elemental composition at a rough surface of the film and figure 6 near the smooth surface.

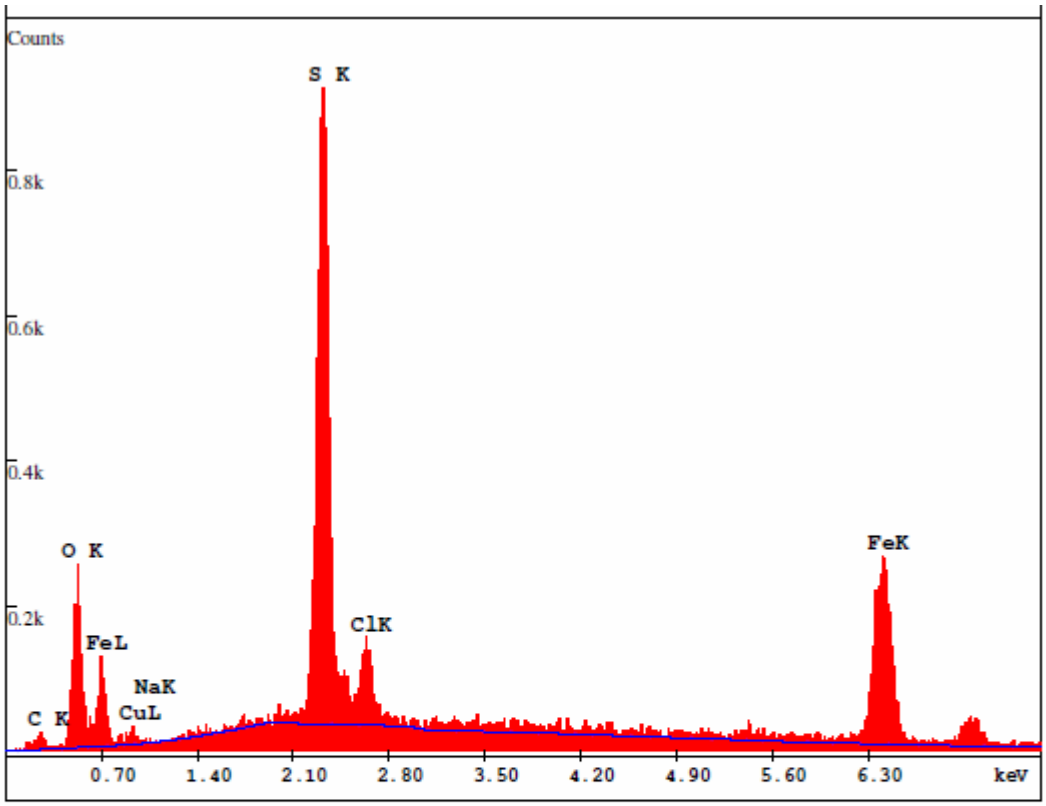


EDAX ZAF Quantification (Standardless)
Element Normalized
SEC Table : User c:\edax32\eds\genuser.sec

| Element | Wt % | At % | K-Ratio | Z | A | F |
|---|---|---|---|---|---|---|
| C K | 0.56 | 2.02 | 0.0011 | 1.2001 | 0.1604 | 1.0003 |
| O K | 5.58 | 15.15 | 0.0300 | 1.1716 | 0.4579 | 1.0025 |
| CuL | 0.78 | 0.53 | 0.0023 | 0.9343 | 0.3120 | 1.0002 |
| NaK | 0.03 | 0.06 | 0.0001 | 1.0989 | 0.3181 | 1.0003 |
| S K | 15.09 | 20.47 | 0.1422 | 1.0935 | 0.8604 | 1.0017 |
| ClK | 2.36 | 2.89 | 0.0212 | 1.0442 | 0.8604 | 1.0014 |
| FeK | 75.61 | 58.87 | 0.7230 | 0.9580 | 0.9981 | 1.0002 |
| Total | 100.00 | 100.00 | | | | |

Figure 5. The SEM-EDX analysis of the surface of the film. This analysis is done on the rough surface of the film, when the image magnification is 2000X.

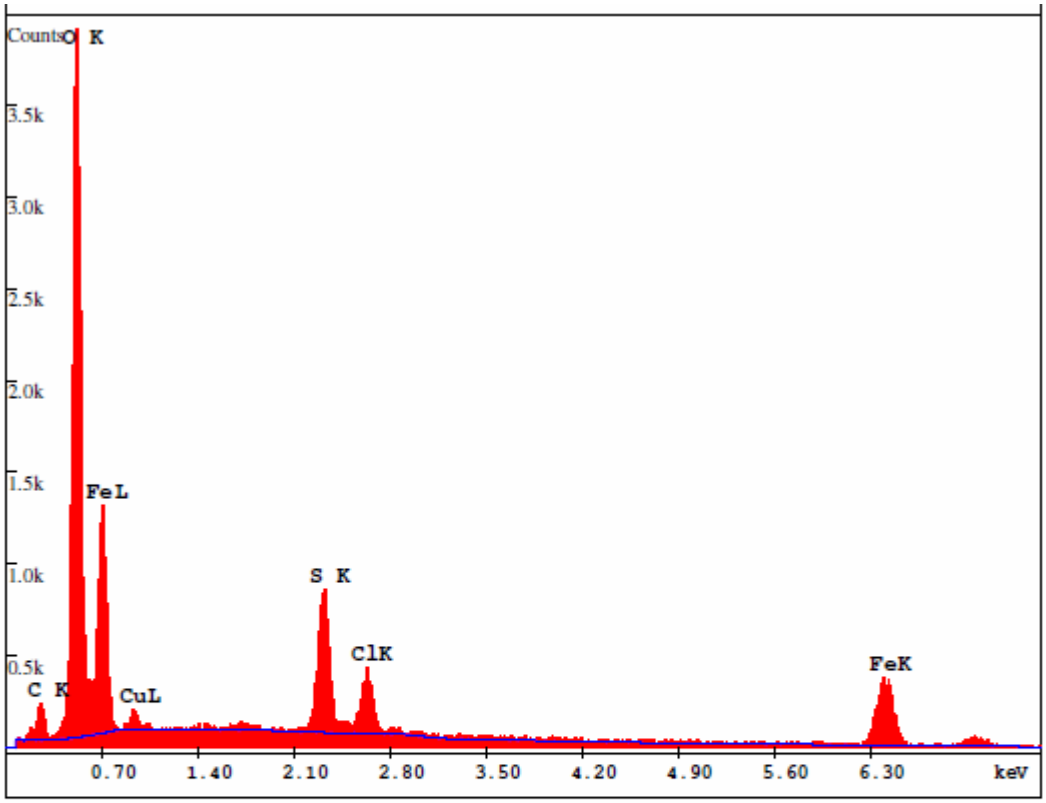


EDAX ZAF Quantification (Standardless)
Element Normalized
SEC Table : User c:\edax32\eds\genuser.sec

| Element | Wt % | At % | K-Ratio | Z | A | F |
|---|---|---|---|---|---|---|
| C K | 2.01 | 4.63 | 0.0050 | 1.1334 | 0.2204 | 1.0004 |
| O K | 35.55 | 61.42 | 0.2256 | 1.1072 | 0.5724 | 1.0013 |
| CuL | 1.81 | 0.79 | 0.0057 | 0.8837 | 0.3592 | 1.0001 |
| S K | 6.10 | 5.26 | 0.0560 | 1.0315 | 0.8880 | 1.0021 |
| ClK | 3.19 | 2.49 | 0.0286 | 0.9844 | 0.9086 | 1.0012 |
| FeK | 51.34 | 25.41 | 0.4608 | 0.8960 | 1.0013 | 1.0005 |
| Total | 100.00 | 100.00 | | | | |

Figure 6. The SEM-EDX analysis of the surface of the film. This analysis was done on a smooth surface of the film when the image magnification was 2000X.